FACT-mediated maintenance of chromatin integrity during transcription is essential for mammalian stem cell viability

Imon Goswami[1, †], Poorva Sandlesh[1, †, &], Aimee Stablewski[2], Ilya Toshkov[3], Alfiya F Safina[1], Mikhail Magnitov[4], Jianmin Wang[5, *], Katerina Gurova[1, *]

[1] Department of Cell Stress Biology, Roswell Park Comprehensive Cancer Center, Buffalo, NY, USA; imon.goswami@roswellpark.org
[2] Transgenic Shared Facility, Roswell Park Comprehensive Cancer Center, Buffalo, NY, USA; aimee.stablewski@roswellpark.org
[3] Buffalo BioLabs, Buffalo, NY, USA; itoshkov@genomeprotection.com
[4] Institute of Gene Biology Russian Academy of Sciences, 119334 Moscow, Russia; mikhail.magnitov@phystech.edu
[5] Department of Biostatistics and Bioinformatics, Roswell Park Comprehensive Cancer Center, Buffalo, NY, USA; Jianmin.wang@roswellpark.org
[&] Present address: Department of Neurological Surgery, University of Pittsburgh, Pittsburgh, PA University of Pittsburgh, Hillman Cancer Institute, Pittsburgh, PA; poorva1@gmail.com

[†] These two authors contributed equally to the work.

**Corresponding authors*: Katerina Gurova, Department of Cell Stress Biology, Roswell Park Comprehensive Cancer Center, Elm and Carlton Streets, Buffalo, NY, USA, 14263. Tel: 716-845-4760, email: katerina.gurova@roswellpark.org, Jianmin Wang, Department of Biostatistics and Bioinformatics, Roswell Park Comprehensive Cancer Center, Buffalo, NY, USA, 14263. Tel: 716-845-1499, email: jianmin.wang@roswellpark.org.

Running Title: FACT preserves nucleosomes during transcription

Keywords: Nucleosome/SPT16/SSRP1/Stem cell/Transcription

Abstract

Preservation of nucleosomes during replication has been extensively studied, while the maintenance of nucleosomes during transcription has gotten less attention. The histone chaperone FACT is involved in transcription elongation, although whether it disassembles or assembles nucleosomes during this process is still unclear. We deleted the FACT subunit in adult mice to clarify the function of FACT in mammals. FACT loss was lethal due to the loss of the earliest progenitors in bone marrow and intestine, while mor differentiated cells were not affected. Using cells isolated from several tissues, we showed that FACT loss was lethal only for stem cells but not cells differentiated *in vitro*. FACT depletion led to increased chromatin accessibility in a transcription-dependent manner, suggesting that nucleosomes are lost during transcription in the absence of FACT. The most prominent response to the loss of nucleosomes was the activation of interferon signaling and the accumulation of immunocytes in sensitive organs. FACT maintained chromatin integrity during transcription in mammalian adult stem cells, suggesting that chromatin transcription in these cells is different from more differentiated cells.

52 **INTRODUCTION**

53 Chromatin organization defines cell identity by limiting the access of transcription machinery to
54 DNA in a region-specific manner, making the existence of cell- and condition-specific
55 transcriptional programs possible. Although significant progress has been made in elucidating
56 the structure and mechanism of action of factors involved in chromatin maintenance, studies
57 have mainly used cell-free conditions or simplified model organisms (e.g., yeast or human
58 tumor cells). The role of these factors in modifying gene expression in a cell-specific manner in
59 multicellular organisms, including the spatio-temporal regulation of their activities, is still far
60 behind.

61 One group of such factors is the histone chaperones that have long been considered a
62 component of the basic replication and transcription machinery responsible for the assembly
63 and disassembly of nucleosomes [1]. However, studies done in multicellular organisms
64 demonstrated that they are not ubiquitously expressed and that their depletion has different
65 consequences for different cells [2-5]. These characteristics suggest that either their function is
66 not unique or the control of chromatin integrity may not be required in all cells.

67 Histone chaperone FACT (FAcilitates Chromatin Transcription) is especially interesting in this
68 regard. In recent years, the view of its function as an essential transcription elongation factor
69 facilitating the access of the transcriptional machinery to nucleosomal DNA has been
70 questioned by several mechanistic and structural studies [6], [7]. FACT does not bind to
71 nucleosomes fully wrapped with DNA but binds to nucleosomes with partially unwrapped DNA
72 [8-10]. Reduced FACT levels in several cell types increase chromatin accessibility at different

genomic regions and are accompanied by elevated transcription [11, 12], suggesting that FACT may restrict the access of the transcriptional machinery to DNA. The phenotypes of FACT knockout in *C. elegans* or *D. rerio* do not support the proposed function of FACT as an essential transcription elongation factor [13, 14]. Different laboratories have demonstrated that several normal mammalian cell types do not depend on FACT for growth or viability [11, 14, 15]; however, most mouse and human tumor cells cannot grow or die after FACT knockdown [12, 16]. It is still not clear what makes tumor cells dependent on FACT. This knowledge could be valuable for cancer research. The absence of FACT expression in most adult mammalian cells [17] suggests that FACT may have cell-specific functions or that some, but not all, cells require FACT due to a specific chromatin state. To understand FACT function in multicellular eukaryotes, it is critical to identify which mammalian cells depend on FACT and which processes are disturbed in these cells upon FACT loss.

FACT consists of two subunits, SPT16 (Suppressor of Ty 16) and SSRP1 (Structure-Specific Recognition Protein 1). General knockout (KO) of the *Ssrp1* gene in mice is lethal at the blastocyst stage [18] when expression of the FACT subunits is the highest in the life span of mice [17]. However, whether FACT is essential for the viability of adult mice when its expression is very low is not known. The stability of both FACT subunits depends on their binding to each other, and depletion of one leads to the disappearance of the other [19]. Based on this knowledge, we generated an *Ssrp1* conditional knockout (KO) mouse model to eliminate FACT and observe cell-specific and age-dependent consequences of FACT loss. Specifically, we crossed mice with LoxP sites inserted into the introns of the *Ssrp1* gene and R26-CreER^{T2} mice to achieve FACT depletion in adult animals using tamoxifen administration [20]. In this study,

95 we determined the phenotypes of FACT loss in mice at different ages and identified the FACT-
96 dependent cells in FACT-sensitive organs. We also propose the reasons for this selective FACT
97 dependency.

98 **Results**

99 **1. FACT loss in mice is lethal at all ages**

100 For this study, we compared mice homozygous for the *Ssrp1* mutant allele, *Ssrp1*$^{fl/fl}$, with
101 heterozygous and wild-type animals [20]. Consistent with a previous report [18] we
102 demonstrated that mice with one functional *Ssrp1* allele lacked any phenotype. Therefore, we
103 used these heterozygous mice as controls in many experiments. These mice were crossed with
104 Rosa26 CreERT2 (*CreER*$^{T2+/+}$) mice to obtain mice homozygous for both alleles since the
105 presence of one copy of *CreER*^{T2} results in poor or no excision of *Ssrp1* [20]. Treatment of the
106 mutant mice with tamoxifen for five days led to the reduction and disappearance of both FACT
107 subunits in the spleen, the only organ in adult mice where SSRP1 and SPT16 can be detected by
108 immunoblotting (Fig.EV1A). Based on this finding, tamoxifen was administered for five days in
109 subsequent experiments.

110 One week after the end of tamoxifen administration, both female and male mice began losing
111 weight and died or were euthanized between 12 and 50 days after the end of treatment
112 (Fig.1A, B). Because Cre can cause DNA damage due to its non-specific recombinase activity, we
113 tested the effect of tamoxifen administration on mice with two CreER^{T2} alleles and wild-type
114 *Ssrp1* and did not observe any toxicity (Fig.EV1B), indicating that FACT loss caused the deaths of
115 *Ssrp1*$^{fl/fl}$ mice. Older male mice (24–40 weeks at the start of tamoxifen administration) lived

116 longer than younger males or female mice; however, they still died after FACT loss (Fig.1B). A
117 comparison of the complete blood counts (CBC) between male and female *Ssrp1*$^{fl/fl}$*; CreER*$^{T2+/+}$
118 mice treated with tamoxifen or vehicle control showed a significantly reduced number of white
119 blood cells (i.e., lymphocytes and granulocytes) but no changes in the numbers of red blood
120 cells and platelets (Fig.1C). Serum biochemistry analysis did not find a significant deviation
121 between tamoxifen treated *Ssrp1*$^{fl/fl}$*; CreER*$^{T2+/+}$ *and Ssrp1*$^{fl/+}$*; CreER*$^{T2+/-}$ mice except slight
122 reduction of lipase in homozygous mice (Table EV1). Tamoxifen-treated *Ssrp1*$^{fl/fl}$*; CreER*$^{T2+/+}$
123 mice showed signs of dehydration, and some animals developed atopic dermatitis-like skin
124 lesions (Fig.1D). Subcutaneous fluids (1-2 mL/day) did not rescue these mice (Fig.EV1C). Thus,
125 although FACT is only present in a limited number of cells in several organs of adult mice [17], it
126 is essential for the viability of adult mice. For subsequent experiments, we used mice between
127 10 and 15 weeks of age.

128 **2. Several tissues are sensitive to FACT depletion**

129 Gross pathology examination revealed complete loss of adipose tissue (Fig. 1E, F) and
130 accumulation of liquid in the large intestine (Fig.1E) following the loss of FACT. The weights of
131 the major parenchymal organs were not significantly changed, except the spleen, which was
132 smaller in the tamoxifen-treated groups (Fig. EV1E). The ovaries were also significantly reduced
133 in the tamoxifen-treated mice (Fig.EV1F); however, these changes have been observed in mice
134 with wild-type *Ssrp1* and reported in the literature as a direct effect of tamoxifen treatment
135 [21]. In contrast, the testes, which also have high FACT expression [17], were not reduced by
136 tamoxifen treatment (Fig.EV1E, G).

137 Upon FACT depletion histological changes were found in organs that express FACT subunits in
138 basal conditions [17]. Reduced cellularity was observed in the bone marrow and spleen,
139 including atrophic changes in the red pulp (Fig.2A), areas where FACT is present in adult mice
140 [17]. High FACT levels are also present in cells at the bottom of the crypts of the small and large
141 intestines [17]. *Ssrp1* KO resulted in the thinning of the colon villi and the emergence of a small
142 number of degenerative crypts (Fig. 2A, B). No histological changes were seen in the high FACT-
143 expressing testes (Fig. EV1G). There was also no reduction in FACT expression in the testes after
144 tamoxifen administration (Fig. EV2A), suggesting that recombination did not occur in the testes,
145 most probably due to the limited penetration of tamoxifen through the blood-testis barrier
146 [22]. Among the FACT-negative organs, tamoxifen administration causes histological changes
147 only in the liver; there was a loss of glycogen granules in the hepatocytes. Some of the
148 hepatocytes were enlarged or undergoing mitosis, which is not typical for the adult liver.
149 Lymphoid cell infiltration was also seen in some areas (Fig.2C). The skin was excluded from the
150 histological analysis in this study because the skin lesions first appeared in mice when they lost
151 almost 20% of their weight, requiring euthanasia. Accurate assessment of the consequences of
152 FACT loss in the skin will require mouse models with keratinocyte-specific expression of
153 $CreER^{T2}$.

154 Altogether these findings may indicate the suppression of hematopoiesis and the suppression
155 of the renewal capacity of the intestine, leading to atrophic changes that could explain the
156 observed dehydration because the large intestine is the major organ of water absorption.
157 Changes in the liver and reduction of lipase concentration in serum are likely secondary to
158 weight loss. The loss of adipose tissue could explain the weight loss and might be either primary

159 (death of adipocytes) or secondary (loss of fat from cells due to malnutrition and dehydration)
160 to FACT loss.

161 **3. FACT loss impairs proliferation and induces cell death in several organs**

162 To better understand the consequences of FACT depletion we compared the levels of
163 proliferation and cell death in the major parenchymal organs between vehicle- and tamoxifen-
164 treated mice using EdU labeling as a marker of DNA replication and cleaved caspase-3 staining
165 as a marker of apoptosis. Three days after the end of tamoxifen treatment, the number of EdU-
166 positive cells was significantly reduced in the spleen and intestines of *Ssrp1*$^{fl/fl}$*; CreER*$^{T2+/+}$ mice
167 (Fig.3A–C). Although EdU-positive cells are normally absent from the liver, some EDU-positive
168 cells did appear following tamoxifen treatment, consistent with the appearance of mitotic cells
169 in the H&E-stained liver sections (Fig.2C and EV2B). Changes in EdU positive cells in the small
170 and large intestines were moderate, with some sections with no changes in the number of EdU-
171 positive cells and some areas with a reduced frequency of replicating cells in the lower portion
172 and the spread of replicating cells towards the upper portion of the crypts (Fig.3B, C). In the
173 spleen, intestines, and colon, we observed a slight increase in the number of cleaved caspase-3-
174 positive cells; however, they were not concentrated in any specific cellular zone in these organs
175 (Fig.3D and EV2C). Thus, FACT depletion reduced the number of cells in the hematological
176 organs and intestines. This loss of cells was predominantly due to reduced cell proliferation of
177 cells. Interestingly, hepatocytes started proliferating in the liver upon *Ssrp1* KO. Thus, a general
178 impairment of DNA replication or mitosis, processes involving FACT activity [23-27], cannot
179 explain the toxicity of *Ssrp1* KO.

180 **4. FACT depletion is accompanied by the loss of long-term hematopoietic stem cells**
181 **from bone marrow and Lgr5 positive stem cells from the intestines**

182 To identify cells sensitive to FACT loss in hematopoietic and intestinal tissues, we performed
183 single-cell RNA sequencing (scRNA-seq). Quality control confirmed the integrity of the samples
184 with viabilities of > 90% and > 75% for the cells obtained from the bone marrow and intestines
185 respectively. There were a comparable number of cells sequenced (about 8,000–10,000 per
186 sample), the number of reads generated (about 20,000–27,000), and the number of genes
187 quantified (approximately 1000 per cell) (Fig. EV3A-B).

188 The Uniform Manifold Approximation and Projection (UMAP) plots for vehicle- and tamoxifen-
189 treated samples showed significant overlap, suggesting that, in general, the tissue architecture
190 was well preserved in both organs (Fig. EV3C). There were no significant changes in the
191 distribution of cells at the different phases of the cell cycle within the clusters between the
192 vehicle- and tamoxifen-treated samples and no preferential depletion of cells in any particular
193 phase of the cell cycle (Fig. EV3D, E), suggesting that FACT loss did not block any specific phase.

194 A comparison of the bone marrow UMAP plots revealed several clusters with visibly changed
195 numbers of cells. Three clusters (14, 15, and 16) almost completely disappeared after FACT
196 depletion (Fig.4A). Using the Immunological Genome Project (ImmGen) database [28] as a
197 reference, we identified the major types of bone marrow cells in our samples (Fig.4B). There
198 were no dramatic differences in the proportions of the different cell types between samples
199 from the vehicle- and tamoxifen-treated mice (Fig. 4C). In several instances, the clusters with
200 increased or decreased numbers of cells belonged to the same cell type (e.g., the disappearing

201 clusters 14–16 and the increasing cluster 9 were all identified as 'stem cells') (Fig.4D). The same
202 was true for the neutrophils and B cells. Several clusters consisting of one cell type (cluster 11 –
203 dendritic cells (DC), 20 – basophils (Bph), 21 – T cells, and 22 – NK cells) were slightly increased
204 in number (Fig. 4C, D). Therefore, we examined the differences between the decreased and
205 increased clusters of the same cell type.

206 In the control samples, stem cells formed two separate groups: a central group isolated from
207 other cells (clusters 14–16) and a group connecting the monocytes and granulocytes (clusters 9,
208 10) (Fig.4B). The central group of stem cells disappeared, while the cluster connecting the
209 granulocytes and monocytes slightly increased (Fig.4B). We used the ImmGen datasets specific
210 for bone marrow stem cells to determine the differences between these subpopulations. We
211 identified 11 types of stem cells in our dataset (Fig.4E). The most dramatic change was
212 observed for the long-term hematopoietic stem cells (LTHSCs), which completely disappeared
213 after *Ssrp1* deletion (Fig.4E, F). $CD34^-$ LTHSCs gave rise to $CD34^+$ LTHSCs (LT34Fs), which
214 increased in number; however, the total cell count was very low and unreliable (one cell in the
215 control and four cells after FACT loss). The LT34Fs were followed by short-term HSCs (ST-HSCs),
216 consisting of ST34Fs ('CD34+Flk2- ST-HSC') and STSLs ('short-term reconstituting stem cell'),
217 whose numbers were slightly reduced or increased upon FACT loss, respectively (Fig.4E, F).
218 Lineage-committed progenitors changed in different directions. For example, the number of
219 multipotent progenitors (MPP34F, CD34+Flk2+ multipotent progenitors) was increased, while
220 the number of committed progenitors changed either up (MLP – multilymphocyte progenitors,
221 CMP – common myeloid progenitors, CDP - common dendritic cell progenitors, GMP -
222 granulocyte-monocyte progenitor) or down (MEP – megakaryocyte- erythroid progenitors, MDP

223 – monocyte dendritic cell progenitors) (Fig. 4E, F). Thus, the stem cells most sensitive to FACT
224 depletion in bone marrow were the earliest hematopoietic progenitors, LTHSCs. Changes in the
225 number of other stem cells may be direct (in case their viability depends on FACT) or secondary
226 (redistribution in response to loss of cells dependent on FACT).

227 To understand the differences in the neutrophils (increased in clusters 1–3, 5; decreased in
228 clusters 6–8), we ran Gene Set Enrichment Analysis (GSEA, MSigDB) using gene markers specific
229 for these clusters (Fig. 4G and Table EV2). We found that FACT loss resulted in more neutrophils
230 expressing genes of the Interferon (IFN) gamma response and induced by other inflammatory
231 cytokines (e.g., TNF and IL-6), while genes expressed in neutrophils that decreased in number
232 were enriched in gene lists for proliferative response and elevated metabolic turnover (Fig. 4F
233 and Table EV2). Common genes between the two sets of clusters were enriched in several
234 neutrophil datasets (Table EV2).

235 We ran the same analysis for B cells by comparing cluster 17 (increased) with clusters 18 and 19
236 (decreased). The total number of B cells increased almost two-fold (6.5% vs. 13.1%, Fig.4C),
237 suggesting that they might migrate from outside the bone marrow. Results of this comparison
238 paralleled the neutrophils (Fig.4H and Table EV2). Upon FACT loss, there were more B cells with
239 a transcriptional program similar to 'Allograft rejection' and 'IFN gamma response,' while in the
240 control bone marrow there were more B cells expressing genes enriched for 'MYC targets,'
241 'G2M checkpoint, and ' E2F targets'. Thus, these data suggest that FACT depletion in
242 neutrophils and B cells resulted in the inhibition of the expression of genes involved in

243 proliferation and metabolism and the induction of genes induced by IFNs and other
244 inflammatory cytokines.

245 Intestine UMAP plots showed that three neighboring clusters were completely lost (Fig.5A,
246 clusters 1–3), while several clusters increased (clusters 10 - 14) or emerged de novo (clusters 4,
247 8, 9, 16, which had no or a very few cells in control sample). To recognize intestinal cells, we
248 used data published by Gao et al. [29] and Haber et al. [30]. All clusters were ascribed to certain
249 intestinal cell types, except cluster 12, which was not identified (Fig. 5B and Table EV3). In most
250 cases, comparison of our data with both published datasets resulted in assignment of cells to
251 the same type. The transcription signature of the most prominently lost cluster (1) included
252 'large intestine Lgr5-positive stem cells' [29]. Cells of this cluster also had high expression of
253 *Gkn3*, a marker of small intestine stem cells [30] (Fig. 5C, D).

254 No other cell types were completely lost upon FACT depletion. Lost clusters 2 and 3 were
255 recognized as small and large intestine enterocyte progenitors using the Gao dataset (Fig. 5B, C)
256 or proximal enterocytes using the Haber dataset (Fig. 5E). However, in the FACT-depleted
257 intestine, similar cells were found within de novo emerged clusters 4, 8, and the increased
258 clusters 9 –11 (Fig.5B, C, E). The close location of the reduced and increased clusters and their
259 similar classification suggested that the enterocyte progenitors did not die upon FACT loss but
260 had their transcriptional program shifted. Thus, we looked for differences in gene markers of
261 clusters 2 and 3 (almost completely lost in the *Ssrp1* KO sample) and clusters 8 and 9 (emerged
262 in the *Ssrp1* KO sample) (Fig. 5F) using GSEA. This comparison showed that FACT depletion in
263 enterocyte progenitors resulted in downregulation of genes involved in 'oxidative

264 phosphorylation,' 'adipogenesis,' ' mTORC1 signaling,' and 'glycolysis,' or being 'MYC targets,
265 while the upregulated genes were part of categories 'IFN gamma and alpha response,'
266 'activated by IL2 via STAT2 signaling,' and 'late estrogen response' (Fig. 5F and Table EV3).
267 Surprisingly, these results were similar to what we observed with bone marrow neutrophils and
268 B cells.

269 There were little changes in the number of cells in clusters 6 and 7 (Fig.5A), composed of distal
270 enterocytes according to Haber or large intestinal enterocytes according to Gao. Quantitation
271 revealed a slight increase in the number of Goblet cells and their progenitors and Paneth cells
272 (Fig. 5B, C). Cluster 13 had an increased number of cells upon FACT loss (Fig.5A). These cells had
273 a gene expression signature for large intestine immune cells (FDR q-value = 9.93 e-65) and were
274 positive for Dclk1, a marker of intestinal Tuft cells (Fig.5E). Changes in intestinal cell
275 composition were similar to those seen in bone marrow, namely the disappearance of the
276 earliest intestinal stem cells and an increase in the number of more mature cell types. Cells in a
277 state between stem and fully differentiated likely respond to FACT loss by reducing
278 proliferation and inducing the IFN response.

279 Thus, scRNA-seq data suggest that the cell types most sensitive to FACT loss are the
280 undifferentiated stem cells. More mature differentiated cells tolerate FACT depletion; however,
281 these findings need to be confirmed by additional methods.

282

283 **Stem cells from several organs cannot expand *in vitro* in the absence of FACT**

284 To confirm that stem cells are dependent on FACT for viability and growth, we compared the
285 colony-forming ability of stem cells from FACT-sensitive organs. Cells isolated from bone
286 marrow, small intestine, and colon were plated in stem cell medium and treated with 4-
287 hydroxytamoxifen (4-OHT, active metabolite of tamoxifen) to induce *Ssrp1* deletion *in vitro*. A
288 similar experiment was performed with mesenchymal stem cells (MSCs) from adipose tissue to
289 determine whether the loss of adipose tissue is a primary or secondary effect of *Ssrp1* KO.
290 While the growth of skin fibroblasts from the tails of the same mice was not affected by *Ssrp1*
291 deletion [12], the growth of all stem cells was significantly reduced. No colonies formed from
292 bone marrow isolated from *Ssrp1*$^{fl/fl}$*; CreER*^{T2} mice in the presence of 4-OHT; however, 4-OHT
293 did not interfere with the growth of bone marrow cells from genotypes not resulting in bi-allelic
294 *Ssrp1* deletions (Fig.6A, B). No organoids formed from the small intestine or colon stem cells
295 from *Ssrp1*$^{fl/fl}$*; CreER*^{T2} mice upon 4-OHT administration (Fig.6C, D). The adipose MSCs were
296 growing in medium with 4-OHT but at a slower rate than the vehicle-treated cells, and their
297 numbers were reduced due to increased apoptosis upon FACT depletion (Fig.6E, H).

298 To determine if cells lose their dependence on FACT for viability upon differentiation, we
299 isolated intestinal and adipose stem cells and grew them under conditions that either
300 maintained their undifferentiated state or induced differentiation *in vitro* [31-33]. For both
301 types of cells, 4-OHT administration was toxic only to undifferentiated cells. Intestinal organoids
302 maintained in the absence of R-spondin 1 differentiated into more mature enterocyte-like cells
303 [31], lost expression of *Lgr5* and became insensitive to FACT depletion (Fig.6 F, G). In the case
304 of the adipose MSCs, we obtained cultures of differentiated adipocytes and osteocytes using
305 specific differentiation media [34] and demonstrated that neither adipocytes nor osteocytes

306 died upon FACT depletion (Fig.6H, I). Thus, only undifferentiated stem cells are dependent on
307 FACT for viability. Consistent with this data, FACT levels decrease upon differentiation (Fig. 6G,
308 J).

309 **5. FACT loss in stem cells leads to significant changes in chromatin accessibility in a**
310 **transcription-dependent manner.**

311 To understand the cause of stem cell loss upon FACT depletion, we investigated the changes in
312 transcription and chromatin structure in adipose MSCs, cells which viability and growth depend
313 on FACT, but which do not die upon FACT loss. First, we compared general transcription in
314 MSCs before and after FACT depletion by measuring the incorporation of modified
315 ribonucleotide 5-Ethynyl Uridine (EU) into newly synthesized RNA. We observed a slight but
316 highly reproducible increase in EU incorporation in cells without FACT compared to those
317 expressing FACT (Fig. 7A, B), suggesting that general transcription was increased in the MSCs
318 upon FACT loss. This phenomenon was not the result of 4-OHT treatment since cells
319 heterozygous for the *Ssrp1*^{fl} allele showed almost identical EU incorporation before and after
320 treatment (Fig. EV4A, B).

321 Next, we performed RNA-seq on samples from MSCs before and after 4-OHT treatment. There
322 was a smaller number of genes for which expression changed in *Ssrp1*$^{fl/+}$ heterozygous cells
323 than in homozygous *Ssrp1*$^{fl/fl}$ cells. There was almost no overlap in the genes whose expression
324 was changed between the homozygous and heterozygous cells in response to 4-OHT (Fig.
325 EV4C), confirming that the gene expression changes in the *Ssrp1*$^{fl/fl}$ cells were in response to
326 FACT loss and not 4-OHT administration. In the homozygous cells, many more genes were

327 upregulated upon FACT loss than downregulated (Fig.7C, D), whereas the changes in the gene
328 expression of heterozygous cells were more random (Fig. EV4C, D).

329 Gene ontology (GO) analysis of the upregulated genes showed that the most significantly
330 enriched category was the interferon response (Fig.7E and Table EV4). The downregulated
331 genes did not have a dominant category but belonged to the 'PI3K-AKT signaling pathway,'
332 'negative regulation of transcription,' 'extracellular matrix (ECM) remodeling,' 'negative
333 regulation of cell differentiation,' and 'positive regulation of cell proliferation' categories (Fig.7F
334 and Table EV4). Many of these categories reflected the observed phenotypic changes in these
335 cells.

336 The chromatin state in the MSCs before and after 4-OHT treatment was analyzed using the
337 Assay for Transposase-Accessible Chromatin with high-throughput sequencing (ATAC-seq) [35].
338 Because cells in different phases of the cell cycle have different degrees of chromatin
339 accessibility, we limited the influence of this factor by maintaining cells for 48 hours in serum-
340 depleted medium after 4-OHT treatment. Profile plots were built for the distribution of ATAC-
341 seq reads at genomic regions flanking all known mouse genes, 3 kb before the transcriptional
342 start site (TSS), 3 kb after the transcription end site (TES), and in between. Transposase inserts
343 adaptors into genomic regions lacking nucleosomes (i.e., nucleosome-free or linker DNA of
344 accessible chromatin). These adapters can be used as primers for PCR amplification. Selection
345 of the length of the amplified fragments allows the identification of nucleosome-free regions
346 (i.e., reads with the length shorter than nucleosomal DNA [< 120 bp]) or regions occupied by
347 one nucleosome (i.e., reads with fragment lengths corresponding to mononucleosomes with

348 linker DNA [>120 and <250 bp]) as described by Buenristro [35]. The profile plots showed very
349 good overlap between replicates of the vehicle- and 4-OHT-treated cells (Fig.8), suggesting high
350 reproducibility of the effect. The plots built from the nucleosome-free and mononucleosome
351 fragments showed increased chromatin accessibility upon FACT depletion around the TSS and
352 at gene bodies (Fig.8A, B). The increase in the gene bodies was more pronounced for the
353 mononucleosome fragments than the nucleosome-free fragments (Fig. 8C, D).

354 To test whether FACT-mediated control of chromatin integrity depended on transcription, we
355 used RNA-seq data to classify the genes based on their expression levels in cells with FACT.
356 First, we identified genes that were not expressed in any of the tested conditions, which
357 consisted of 26,577 genes out of the 55,401 total mouse genes analyzed. The remaining 28,824
358 genes were divided into four quantiles based on their average expression levels in cells with
359 FACT. The most dramatic change was seen with the top 25% of the expressed genes, for which
360 chromatin accessibility was significantly increased around the TSS and at gene body (Fig.7D).
361 The differences were gradually reduced from the 5' to 3' ends and behind the TES. The
362 differences were also reduced with the reduction in transcription but remained significant for
363 the three top quantiles of the transcribed genes independent of whether nucleosome-free or
364 mononucleosome fragments were analyzed (Fig.8E, F).

365 The differences in chromatin accessibility were not seen for the bottom 25% of the expressed
366 and unexpressed genes when we analyzed the nucleosome-free fragments, while the plots for
367 the mononucleosome fragments for the same categories of genes at the gene bodies were
368 even reverted (i.e., FACT loss caused a slight reduction in chromatin accessibility at the gene

369 bodies with very low or no transcription). To quantify these effects, we compared the mean
370 read density at the gene bodies (excluding the region immediately after the TSS; see the
371 Materials and Methods for details) for the different categories of genes and fragment lengths
372 (Fig.8G). This analysis confirmed there were fewer mononucleosome fragments at poorly
373 transcribed genes upon FACT loss.

374 Untranscribed genes constitute more than half of all the genes used for the analysis and may
375 represent other non-transcribed regions that constitute most of the genome in mammals. Thus,
376 we used a Hoechst 33342 to measure the overall effect of FACT loss on chromatin accessibility.
377 Hoechst 33342 is a cell-permeable minor groove binding molecule whose fluorescence is many-
378 fold increased when bound to DNA. An access of small molecules to the minor groove of DNA is
379 limited when DNA is wrapped around nucleosomes [36, 37]. We incubated FACT-positive and
380 negative adipose MSC cells with Hoechst 33342 and then measured the fluorescence of
381 individual cells using flow cytometry. To avoid potential differences in the amount of DNA per
382 cell due to different cell cycle phases, we arrested all cells in G1 by serum withdrawal for 48
383 hours. As a positive control, we used the small molecule curaxin CBL0137, which disrupts
384 DNA/histone interactions in cells [9]. As expected, curaxin treatment significantly increased the
385 fluorescence of both homozygous and heterozygous cells (Fig. EV5A). The same effect was
386 observed after 4-OHT treatment of homozygous but not heterozygous cells (Fig.8H and EV5B).

387 Thus, FACT loss resulted in increased chromatin accessibility, the degree of which was
388 dependent on the level of transcription. The increase in both nucleosome-free and

389 mononucleosomal fragments was likely due to the opening or partial unwrapping and loss of
390 nucleosomes.

391 **Discussion**

392 Transcription research has mainly focused on how RNA polymerase accesses nucleosomal DNA
393 and what factors facilitate this process. FACT has been viewed as a factor facilitating
394 transcription through chromatin [38]; however, accumulating data questions FACT's role in
395 opening nucleosomes to RNA polymerase (reviewed in [39, 40]). These data may be
396 summarized as follows: (i) there is no evidence that FACT removal from eukaryotic cells results
397 in inhibition of transcription, while it has been shown that FACT depletion in several model
398 systems results in no change or even an increase in the absolute transcription levels [12, 16]; (ii)
399 there is no strong data that FACT can bind and destabilize nucleosomes with fully wrapped
400 DNA; however, there is data indicating that FACT binds all nucleosomal components and
401 nucleosomes not fully wrapped with DNA (reviewed in [40]); (iii) decreased FACT levels in cells
402 results in loss of histones from chromatin [41-43] and increased accessibility of chromatin [11].
403 These observations led to the emergence of a new model for the role of FACT in transcription:
404 FACT binds the components of nucleosomes, histone dimers/tetramers, and possibly DNA, to
405 preserve nucleosomes at their positions during RNA polymerase passage; without FACT,
406 nucleosomes are prone to disassembly by transcription machinery or associated factors. This
407 model can also explain the initially puzzling observation that while FACT enrichment at
408 mammalian genes is highly proportional to the transcription level, the transcription of genes
409 bound by FACT is not inhibited by FACT removal [12, 15, 44]. The greater the transcription

410 levels (i.e., more frequent passage of RNA polymerase through a region), the more frequently
411 nucleosomes are disturbed and the more opportunities for FACT to bind. As previously
412 demonstrated, the re-establishment of histone-DNA contacts displaces FACT because of the
413 higher affinity of histones for DNA than for FACT [45]. Therefore, genes with lower transcription
414 (i.e., less frequent passage of RNA polymerase) accumulate less FACT. At the same time, if FACT
415 loss is accompanied by the loss of nucleosomes from the transcribed region, we might expect
416 an facilitated passage of RNA polymerase through this region in the absence of nucleosomes,
417 i.e. elevated transcription.

418 In this study, we tested and confirmed this proposed model in a mammalian system. Although
419 in this study we genetically excised only *Ssrp1* gene, we have never observed in mammalian
420 cells existence of SPT16 in the absence of SSRP1 and unbound to SSRP1. Thus, we discuss below
421 the consequences of the loss of the whole complex rather than SSRP1 subunit, though
422 theoretically SSRP1 may have independent activity in some cells or conditions.

423 We demonstrated that FACT is the major factor responsible for the maintenance of chromatin
424 during transcription and is essential for the viability of a small fraction of cells in adult mice.
425 However, these cells are vital to the viability of adult mice because *Ssrp1* KO was lethal for mice
426 at all tested ages (5–40 weeks). Together with previously published data that general *Ssrp1* KO
427 is lethal at 3.5 dpc [18], our new data revealed that *Ssrp1* is an essential gene in mammals
428 because it is critical for the survival of stem cells. Since we did not use aged mice in our
429 experiments, consequences of FACT loss in geriatric animals requires further investigation.

430 The hematopoietic and intestinal tissues were the most sensitive to FACT loss. Both tissue types
431 are dependent on the constant replenishing of cells from tissue-specific stem cells. The earliest
432 progenitors in both systems were completely lost upon *Ssrp1* KO. The stem cells in other tissues
433 may also be sensitive to FACT loss, as indicated by the depletion of adipose tissue and the
434 presence of skin abnormalities. For testing the role of FACT in the viability of other tissues,
435 tissue-specific *Ssrp1* KO is needed to prevent the death of animals from the bone marrow and
436 intestinal failure.

437 FACT is not essential for many types of adult cells [12, 16]. Here, we established that number of
438 many cell types, mostly differentiated but also some progenitors, increased upon FACT loss.
439 This increase is likely due to FACT-independent, compensatory redistribution of cell
440 populations; however, time-dependent monitoring of organ cell composition upon *Ssrp1* KO is
441 needed to establish this. In addition, the abundance of these cell types, even among stem and
442 progenitor cells, suggests that multiple adult cells do not need FACT for survival. Importantly,
443 there were many proliferating cells among the FACT-independent cell types. We also did not
444 see changes in the cell-cycle distribution upon FACT loss, suggesting that stem cells disappear
445 not due to problems with replication or mitosis, processes where FACT activity has been
446 observed [23, 27]. Thus, an important question is what makes these cells sensitive to FACT loss.
447 To address this question, we showed that FACT loss resulted in a significant increase in
448 chromatin accessibility. Previously, we observed that FACT removal from differentiated
449 fibroblasts, which express low FACT levels and are not sensitive to *Ssrp1* KO, does not lead to
450 the loss of nucleosomes, while it does in oncogene-transformed cells [12]. Therefore, we
451 propose that there is a specific chromatin state in some stem cells and oncogene-transformed

452 cells, where nucleosomes are not as stable as in other cells what makes these nucleosomes as
453 well as viability of cells dependent FACT.

454 There is a clear difference between the sensitivity of chromatin to FACT loss depending on
455 transcription, i.e., the higher the transcription rate, the greater the increase in chromatin
456 accessibility upon FACT removal for most of transcribed genes (top 75% of genes). These
457 changes were in line with the increase in global transcription in MSCs upon FACT depletion.
458 However, there was a small but highly significant reduction in chromatin accessibility at
459 untranscribed genes or those with low transcription rates upon FACT loss (at least if comparing
460 mononucleosome fragments). This finding could potentially be explained by the role of FACT in
461 preventing the stalking of folded nucleosomes through binding to the acidic patches [46]. In this
462 case, the loss of FACT in the absence of transcription might lead to a tighter interaction
463 between nucleosomes, leaving fewer opportunities for transposase to invade the linker DNA.

464 An interesting observation that may shed light on the physiological consequences of chromatin
465 destabilization is the increase in the number of immune cells in the bone marrow and intestine.
466 The increase in B cells in bone marrow may be due to a shift in differentiation, whereas the
467 number of T cells in the bone marrow and intestine may only be increased due to migration.
468 This accumulation may be related to the fact that the most upregulated pathway in response to
469 *Ssrp1* KO in all cell systems examined was the IFN response. We previously observed activation
470 of the IFN response in mice treated with curaxin CBL0137, which disrupts histone/DNA binding
471 [9]. IFNs are well-established factors that attract immune cells to the sites of viral invasion and
472 inflammation [47]. The mechanism of interferon activation upon chromatin destabilization is

473 not fully established; however, in the case of curaxin, it resulted from dsRNA accumulating in
474 cells due to the transcription of pericentromeric repeats [48]. The same mechanism may be
475 involved in the effects of FACT depletion along with other mechanisms, such as the emergence
476 of cryptic initiation from uncapped RNA sensed by the RIG/MAVS5 pathway [49] or the binding
477 of nuclear cGAS to DNA losing nucleosomes [50].

478 In this study, we established that FACT performs a unique function in the earliest progenitor
479 stem cells in several organs of adult mammals. We propose that in these cells, FACT is critical
480 for the maintenance of chromatin during transcription. Loss of FACT results in the loss of
481 nucleosomes at transcribed genes and elevated transcription. The most significantly
482 upregulated pathway in response to the increased chromatin accessibility is interferon
483 signaling, which is likely responsible for the accumulation of immune cells in the sensitive
484 organs in response to FACT loss.

485

486 **Materials and Methods**

487 **Reagents:**

Reagent	Source	Catalogue #	Application
Chemicals and Kits			
DMEM-High Glucose with Pyruvate And L-Glutamine	Corning	MT 10-013-CV	Cell culture
0.05% Trypsin EDTA	Corning	MT 25-052-Cl	Cell culture
10,000U Penicillin-Streptomycin	Corning	MT 30-002-CI	Cell culture
FBS, USDA, Regular, Heat Inactivated	Corning	MT 35-011-CV	Cell culture
α-MEM	Stem Cell Technologies	36450	Cell culture
Advanced DMEM/F-12	Gibco	12634010	Intestinal organoid culture
GlutaMAX™ Supplement	Gibco	35050061	Intestinal organoid culture
lscove's Modified Dulbecco's Medium (IMDM) with L-Glutamine	Gibco	MT 10-016-CV	Bone marrow colony-forming assay
MethoCult™ GF M3434	Gibco	03434	Bone marrow colony-forming assay

KnockOut DMEM	Gibco	10829018	mESC cell culture
Complete Protease Inhibitors – Cocktail, Tablets	Roche	04693132001	Preparation of protein extracts
Laemmli sample buffer	BioRad	1610737	Sample preparation for immunoblotting
Quick Start ™ Bradford 1x dye reagent	BioRad	500-0204	Measurement of protein concentrations
4–20% gradient precast gels	BioRad	4561094	PAGE
PVDF membranes	BioRad	1620177	Immunoblotting
Western Lightning Plus-ECL	PerkinElmer	NEL104001EA	Enhanced chemiluminescence for immunoblotting
Hoechst 33342	Invitrogen	H3570	DNA staining
4-Hydroxytamoxifen	Millipore Sigma Aldrich	H7904-5MG	Induction of Ssrp1 deletion (in vitro)
Tamoxifen	Millipore Sigma Aldrich	T5648-1G	Induction of Ssrp1 deletion (in vivo)
Caspase-3 substrate (Ac-DEVD-AMC)	Enzo Life Sciences	ALX-260-031-M001	Apoptosis assay
Click-iT™ EdU Alexa Fluor™ 488/594 imaging kit	Thermo Fischer Scientific	C10337	Measurement of DNA replication

Click-iT™ EU Alexa Fluor™ 488/594 imaging kit	Thermo Fischer Scientific	C10632	Measurement i=of general transcription
Alizarine Red S	Millipore Sigma Aldrich	A5533-25G	Staining of differentiated osteocytes
Oil Red O	Millipore Sigma Aldrich	O0625-25G	Staining of differentiated adipocytes
Methylene blue	Millipore Sigma Aldrich	M4159	Measuring cell viability
Resazurin sodium salt	Millipore Sigma Aldrich	R7017-1G	Measuring the viability of intestinal organoids
Collagenase A	Millipore Sigma Aldrich	10103578001	Isolation of fibroblasts and mesenchymal stem cells
Dexamethasone	Millipore Sigma Aldrich	D4902	Differentiation of mASCs
Isobutylmethylxanthine (IBMX)	Millipore Sigma Aldrich	I5879-100MG	Differentiation of mASCs
Insulin	Gibco	12585014	Differentiation of mASCs
β-glycerophosphate	Millipore Sigma Aldrich	50020-100G	Differentiation of mASCs
L-ascorbic acid	Millipore Sigma Aldrich	A92902-25G	Differentiation of mASC
Gentamycin	Gibco	15710064	Culturing of intestinal organoids
Murine recombinant EGF	PeproTech	315-09	Culturing of intestinal organoids

Murine recombinant Noggin	PeproTech	250-38	Culturing of intestinal organoids
Human recombinant R-Spondin-1	PeproTech	120-38	Culturing of intestinal organoids
Matrigel	BD Biosciences	356237	Culturing of intestinal organoids
Valproic acid sodium salt	Millipore Sigma Aldrich	P4543-10G	Culturing of intestinal organoids
GSK3 inhibitor CHIR99021	Reprocell	04-0004	Culturing of intestinal organoids
Nextera kit	Illumina	FC-121-1030	ATAC-seq
NEBNext High-Fidelity 2X PCR Master Mix	New England Biolabs	M0541	ATAC-seq
MinElute PCR Purification kit	Qiagen	28004	ATAC-seq
mRNA HyperPrep kit	KAPA BIOSYSTEMS	KK8580	RNA-seq
Antibodies			
SSRP1 mouse monoclonal 10D1	BioLegend	609702	Immunoblotting: 1:3000 Immunohistochemistry: 1:200
SPT16 monoclonal mouse 8D2	BioLegend	607002	Immunoblotting: 1:1000
beta-actin mouse monoclonal (HRP	Millipore Sigma Aldrich	A3854	Immunoblotting 1:20,000

conjugated)			
Mouse Lgr5/GPR49 Antibody	R&D Systems	MAB8240-SP	Immunohistochemistry: 1:200
Cleaved caspase 3	Thermo Fisher Scientific	**700182**	Immunohistochemistry: 1:200
m-IgGκ BP-HRP	Santa Cruz Biotechnology	sc-516102	Immunoblotting: 1:4000
Secondary anti-mouse Alexa Fluor® (488 and 594)	Life Technologies	A-11062 and 11001	Immunohistochemistry: 1:500

488

489 The 10 mg/mL tamoxifen solution was prepared by mixing 100 mg tamoxifen powder in 100 μL
490 99% proof ethanol and then slowly dissolving this in 9.9 mL sterile corn oil at 37°C overnight. A
491 5 mM stock solution of 4-hydroxytamoxifen (4-OHT) was prepared by dissolving 4.8 mg 4-OHT
492 powder in 2.5 mL 99% proof ethanol.

493 Alizarin Red S was prepared by dissolving 2 g powder in 100 mL distilled water. The pH of the
494 solution was adjusted to 4.1–4.3 with 10% ammonium hydroxide. The solution was stored at
495 4°C away from light.

496 Oil red O stock solution was prepared by dissolving 0.7 g powder in 200 mL isopropanol, stirring
497 overnight, and filtering through a 0.2-μm filter. The solution was stored at 4°C away from light.
498 The working solution was prepared fresh by diluting six parts oil red O stock into four parts

499 distilled water. The mixture was incubated at room temperature for 20 min and filtered
500 through a 0.2-μm filter.

501 A 2.5 mM resazurin solution (36X) was prepared by dissolving 0.629 g resazurin sodium salt
502 (Milipore Sigma) in Dulbecco's phosphate-buffered saline (DPBS) and sterilizing through a 0.22
503 μm filter. The solution was stored at -20°C protected from light. The working solution was
504 prepared by diluting this stock to 6X. The working solution was stored at 4°C protected from
505 light for up to 3 months. The 6X solution was used at a final concentration of 70 μM.

506 **Animal experiments**

507 **Animal breeding and treatment:** All animal breeding, procedures, and experiments were
508 conducted in accordance with the Institute Animal Care and Use Committee (IACUC) at Roswell
509 Park Comprehensive Cancer Center under an approved IACUC protocol. Mice were maintained
510 in the Laboratory Animal Shared Resource with controlled air, light, and temperature conditions
511 and fed ad libitum with 5% fat chow with free access to water.

512 The conditional FACT Knockout mouse model with the following genotypes were generated as
513 previously described [20]: *SSRP1*$^{fl/fl;}$ *CreERT2*$^{+/+}$ (KO mice), SSRP*1*$^{+/+}$*; CreERT2*$^{-/-}$ (wild type),
514 *SSRP1*$^{+/+}$*; CreERT2*$^{+/+}$, *SSRP1*$^{fl/fl}$*; CreERT2*$^{-/-}$, *SSRP1*$^{fl/fl}$*; CreERT2*$^{-/-}$, and *SSRP1*$^{fl/+}$*; CreERT2*$^{+/-}$
515 (controls).

516 Mice of different ages were treated with 100 μl of tamoxifen (1 mg) or vehicle by daily IP
517 injection for five days. In some experiments, mice received daily subcutaneous injections of
518 0.9% saline (1 mL). Mouse weights and cage-side observations were recorded daily. Animals

519 were euthanized by CO_2 asphyxiation and cervical dislocation upon losing 20% of their body
520 weight. All cells, tissues, and organs were harvested under sterile conditions.

521 **Mouse tissue collection and staining:** Mouse tissues were harvested and preserved in 10%
522 buffered formalin. Paraffin-embedded tissue sections (5 µm) were stained with hematoxylin
523 and eosin (H&E) and anti-SSRP1 and Anti-cleaved caspase-3 antibodies in the
524 Immunohistochemistry Laboratory of the Roswell Park Pathology Resource Network using
525 standard techniques. All slides were scanned using the Aperio system (Aperio Technologies,
526 Inc). Images were collected using Image Scope software (Aperio Technologies, Inc).

527 EdU staining was performed three days after the end of tamoxifen treatment. Briefly, mice
528 were injected with 50 mg/kg EdU (Invitrogen, Thermo Fisher Scientific) one hour before
529 euthanasia. Tissue sections were stained using the Click-iT EdU Alexa 488 Fluor Imaging kit
530 (Thermo Fisher Scientific) and counterstained with 4',6-diamidino-2-phenylindole (DAPI) (Life
531 Technologies) following the manufacturer's instructions. The stained samples were examined
532 using a Zeiss AxioImager A1 microscope equipped with an epifluorescent light source. Images
533 were captured with an AxioCam MRc digital camera and processed with Zeiss Axio Imager Z1
534 microscope software (Carl Zeiss, Germany).

535 **Magnetic resonance imaging (MRI):** Two mice of each gender and genotype were imaged. MRI
536 was performed on day 0 before treatment and days 6, 8, and 10 after the start of treatment
537 with tamoxifen or vehicle. Images were acquired on a 4.7 Tesla preclinical MRI scanner using
538 the ParaVision 3.0.2 platform (Bruker Biospin, Billerica MA). A 72-mm (ID) quadrature RF coil
539 was used to capture the volumetric data for the entire mouse body. Two NMR tubes filled with

540 1 mM and 3 mM CuSO4 in 1% agarose were included in each session for signal normalization.
541 Following the scout scans, a three-dimensional, fast spin echo scan was acquired using the
542 following parameters: TE/TR = 6.2/100 ms; echo train length = 4; averages = 4; FOV = 113 x 55 x
543 35 mm; matrix = 256 x 128 x128; zero-filled to achieve an isotropic voxel size of 273 microns.
544 Image signal intensities were normalized by a three-point correction curve using two phantoms
545 and background noise, and the whole-body volume was segmented and calculated using the
546 region-growing tool in Analyze 7.0 software (AnalyzeDirect, Overland Park KS). Adipose tissue
547 was segmented from lean tissue using a fixed intensity threshold derived from the average
548 threshold of all datasets, as reported by the Otsu method (REF) and confirmed by visual
549 inspection. The percent adipose tissue volume was calculated as a ratio of voxels segmented as
550 adipose tissue divided by the total body voxels.

551 **Complete blood counts (CBC) and serum biochemistry:** Blood (50 μL) was collected from the
552 saphenous veins of mice before treatment (baseline) and on days 7 and 12 after the start of
553 tamoxifen treatment, as previously described [51]. For serum biochemistry, blood was collected
554 from deeply anesthetized mice via cardiac puncture into serum separator tubes (Sarstedt). The
555 samples were clotted at room temperature for at least 15 min and then centrifuged at 10,000
556 RCF for 10 min. The serum was analyzed using an IDEXX Catalyst DX Chemistry Analyzer (IDEXX
557 Laboratories).

558 **Cells**

559 **Mesenchymal stem cells (MSCs).** MSCs were harvested from the adipose tissue of 8–10-week-
560 old mice. The tissue was minced and digested for 30 min via shaking in a solution of 2 mg/mL

561 collagenase A in PBS at 37°C. The digested tissue was filtered through a 40-μm strainer and
562 centrifuged at 300 g for 5 min. The cells were resuspended in DMEM with 10% FBS and 1%
563 penicillin-streptomycin and plated. To differentiate the MSCs into adipocytes and osteocytes,
564 MSCs were plated on 60-mm plates. When cells reached 80% confluence, differentiation into
565 adipocytes was induced by incubating the cells in medium containing 250 nM dexamethasone,
566 66 nM insulin, and 0.5 mM isobutylmethylxanthine (IBMX) for 21 days. Differentiation into
567 osteocytes was induced by incubating in medium containing 0.1 μM dexamethasone, 10 mM β-
568 glycerophosphate, and 50 uM L-ascorbic acid for 14 days. The differentiation media were
569 changed every 2–3 days. Differentiation into adipocytes and osteocytes was determined by
570 staining with Oil Red O and Alizarin Red, respectively. After differentiation, the cells were
571 treated with 2 μM 4-OHT for five days, and viability was assessed by resorufin staining.

572 Staining for adipocyte and osteocyte differentiation (Oil Red O and Alizarin Red S, respectively)
573 was done by removing the medium, washing cells with PBS, and fixing with 10% neutral
574 buffered formalin for 30 min with gentle shaking at room temperature. The cells were washed
575 twice with distilled water, and then 60% isopropanol was added to the cells for 5 min. The cells
576 were incubated with the appropriate stain for 20–45 minutes at room temperature, protected
577 from light. The plates were then washed twice with distilled water. The cells were covered with
578 water, and images were taken with a light microscope.

579 **Intestinal stem cell isolation and organoid culture.** Intestinal stem cells were collected as
580 previously described [52]. Briefly, approximately 15 mm of the intestines (small, immediately
581 before cecum; large, immediately after cecum; cecum excluded) was harvested from mice and

582 placed in cold PBS. The intestine was cut open longitudinally and flushed with cold PBS multiple
583 times to remove all the contents. The tissue was cut into 5-mm pieces and incubated at 4°C in
584 PBS containing 2 mM EDTA and 50 μg/mL gentamycin with gentle shaking for 30 min. The tissue
585 was then resuspended in cold PBS and vigorously shaken to dislodge the crypts. After allowing
586 the suspension to settle by gravity for 5 min, the supernatant containing the villus fraction was
587 discarded. The tissue was resuspended in cold PBS and shaken vigorously to enrich the
588 supernatant with the crypt fraction. The crypt fraction was filtered through a 70-μm strainer
589 and centrifuged at 200 g for 3 min at 4°C. The pellet was resuspended in crypt culture medium
590 (advanced DMEM:F12 containing 2% FBS, 50 μg/mL gentamycin, 2 mM L-glutamine, 50 ng/mL
591 EGF, 500 ng/mL R-Spondin-1, 100 ng/mL Noggin, 1 mM valproic acid sodium salt, and 3 μM
592 GSK3 inhibitor CHIR99021. The crypts were counted using a hemocytometer, and 500 crypts
593 were mixed with 50 μL Matrigel at 4°C and pipetted into the center of the wells of 24-well
594 plates prewarmed to 37°C. The domes were allowed to set for 10 min in a 37°C incubator, and
595 then crypt culture medium (500 μL) was gently added to each well. Organoids formed over 7–
596 10 days, with medium changed every 2–3 days. The crypts were passaged as previously
597 described [52]. After two passages, the organoids were treated with 2 μM 4-OHT for five days.
598 On day 6, the organoids were split into new wells and allowed to grow for 5–7 days. The ability
599 to form colonies was assessed by counting the number of organoids in the control- and 4-OHT-
600 treated wells. The data were normalized to the number of colonies formed in the control wells.

601 To differentiate the organoids, the intestinal stem cells were cultured in medium without R-
602 Spondin-1 for 2.5 days as previously described [31]. The undifferentiated organoids were
603 maintained in medium containing R-Spondin-1. The differentiated and undifferentiated

604 organoids were treated with 2 μM 4-OHT for five days, and viability was tested at the end of
605 treatment using resorufin staining.

606 For immunofluorescence, the organoids were fixed in 4% paraformaldehyde (PFA) for 30 min,
607 which partly dissolved the Matrigel. The organoids were collected by centrifugation at 2000
608 rpm for 5 min at room temperature. The pellets were washed with PBS, and the organoids were
609 permeabilized with PBS containing 0.1% Triton X-100 and 3% bovine serum albumin at room
610 temperature with rotating. The samples were then blocked in PBS containing 0.05% Triton X-
611 100 and 1% BSA for one hour with rotating. The organoids were stained with primary
612 antibodies (SSRP1 [1:200], Lgr5 [1:200]) at 4°C overnight with rotating. The organoids were
613 washed with blocking solution and incubated for 1 hr at room temperature with the following
614 secondary antibodies: anti-rat Alexa Fluor 488 (1:500) against Lgr5 and anti-mouse Alexa Fluor
615 594 (1:500) against SSRP1. The organoids were washed with blocking solution and PBS and then
616 counterstained with Hoechst (1:2000 in PBS) for 30 min at room temperature with rotation,
617 protected from light. After staining, the organoids were washed with PBS and then plated in 96-
618 well plates. Images were taken using a Zeiss Axio Imager Z1 microscope (Carl Zeiss, Germany).

619 **Bone marrow colony-forming assay.** The femurs and tibias of mice were excised from the
620 hindlimbs by removing the muscles and connective tissue and cleaned with 70% ethanol. The
621 bones were crushed using a sterile mortar and pestle in PBS to generate a single cell suspension
622 that was filtered through a 70-μm cell strainer. This process was repeated until the bones
623 appeared white, indicating all the marrow was removed. The cells were counted using a
624 hemocytometer, and a suspension containing 4.5 x 10^5 nucleated cells/mL was prepared.

625 Complete IMDM medium was prepared by adding 20 mL IMDM to 80 mL MethoCult M3231. 4-
626 OHT (2 μM) or DMSO (control) was added to 4.1 mL complete IMDM by inverting the tube and
627 vortexing for 5 sec twice. The tube was placed in a refrigerator for 5 min to allow bubbles to
628 escape. The 4.5 x 10^5 cells/mL bone marrow cell suspension (400 μL) was added to each tube of
629 medium and the 4-OHT and control mixtures. The tubes were mixed gently by inverting the
630 tube two times and vortexing three times for 8 sec each at maximum speed, followed by bubble
631 release. The cell + medium + 4-OHT or control mixture (1 mL) was plated in 35-mm dishes using
632 a primed 5-mL syringe with a 19G needle. The final cell density was 40,000 per plate. The plates
633 were incubated at 37°C, and colonies were allowed to form on methylcellulose in the presence
634 or absence of 4-OHT for seven days.

635 **Viability assays**

636 For the methylene blue assay, 0.5% methylene blue in 50% methanol was added to plates after
637 removing the medium. The plates were incubated for 15 min at room temperature with gentle
638 shaking. The plates were washed with distilled water and air-dried. The dye was eluted for 30
639 min at room temperature with 1% sodium dodecyl sulfate (SDS) in PBS with shaking. The
640 absorbance was read at 595 nm.

641 The resorufin assay was used to measure the viability of the intestinal organoids.
642 Undifferentiated and differentiated Intestinal organoids were treated with or without 2 μM 4-
643 OHT for five days in 96 well plates (100 μL). After treatment, 20 μL 6X resorufin solution was
644 added to each well for a final concentration of 70 μM, and the plates were incubated at 37°C
645 for 6 hr. The absorbance was read at 570 nm.

646 **EdU staining**

647 Three days after the last treatment with vehicle or tamoxifen, 50 mg/kg EdU was administered
648 intraperitoneally to the mice. After two hours, the mice were euthanized, and the tissues were
649 harvested and snap-frozen. Tissue sections were fixed with 3.7% paraformaldehyde for 15 min
650 at room temperature. For EdU treatment of cells, the cells were treated with 2 μM 4-OHT for
651 five days and then split. After 24 hr, the cells were incubated with 20 μM EdU for 1 hr. The cells
652 were then fixed with 3.7% PFA in PBS for 15 min at room temperature. Cells and tissue sections
653 were permeabilized with 0.1% Triton X-100 in PBS for 20 min at room temperature. The
654 incorporated EdU was detected using the Click-iT® Plus EdU Imaging Kit (Invitrogen), according
655 to the manufacturer's instructions.

656 **EU staining**

657 MSC cells were treated with vehicle or tamoxifen for five days and then split. After 24 hr, the cells were
658 treated with 0.2 mM EU for 1 hr. After the incubation, the cells were trypsinized, harvested, and washed
659 with PBS in 1% BSA. The cells were fixed with 100 μL Click-iT fixative for 15 min at room temperature.
660 The cells were stained with an SSRP1 antibody using a standard protocol and then for EU according to
661 the manufacturer's instructions. The cells were counterstained with Hoechst 33342. Cell staining was
662 analyzed by flow cytometry.

663 **Immunoblotting**

664 Cells were washed with PBS and lysed on ice with RIPA buffer (150 mM sodium chloride, 1.0%
665 NP-40, 0.5% sodium deoxycholate, 0.1% sodium dodecyl sulfate, and 50 mM Tris, pH 8.0)
666 containing protease inhibitor (Roche) for 30 min. The extracts were centrifuged at 13000 rpm

667 for 15 min to remove the debris. The protein concentrations of the supernatants were
668 determined using Quick Start™ Bradford 1x dye reagent. Equal amounts of protein were boiled
669 with Laemmli buffer at 100°C for 5 min. The samples were briefly centrifuged and then
670 separated on precast 4–20% gradient gels. The proteins were transferred to PVDF membranes,
671 which were blocked with 5% skim milk at room temperature for one hour with gentle shaking.
672 The blots were incubated with primary mouse SSRP1 or SPT16 antibodies at 4°C overnight.
673 After the incubation, the blots were washed and incubated with HRP-conjugated, anti-mouse
674 secondary antibodies for 1 hr at room temperature. As a control, the blots were incubated with
675 HRP-conjugated mouse β-actin antibody at room temperature for 1 hr. The blots were washed
676 for 1 min with Western Lightning Plus- ECL, and images were acquired using the BioRad
677 ChemiDoc™ Touch Imaging System.

678 **Caspase-3 assay**

679 The caspase-3 fluorogenic substrate Ac-DEVD-AMC was reconstituted in DMSO at a
680 concentration of 1 mg/mL. Cells were lysed with 1X CCLR buffer, and the protein concentration
681 was estimated using the Pierce BCA assay. The protein was used at a concentration of 2 μg/μL
682 (50 μL). Ac-DEVD-AMC (20 μM in 20 mM HEPES, 10% glycerol, and 2 mM DTT) was added to
683 each sample in a 96-well black plate (BD Falcon). The plates were incubated at 37°C for 1 hr,
684 and then the fluorescence was measured.

685 **DNA minor groove binding**

686 Cells (500,000) were treated with 4-OHT for five days and then serum-starved (0.5% FBS) for 48
687 hr. For the positive control, cells were treated with 1 μM of CBL0137 for 30 min. The cells were
688 washed with PBS and stained with 3 μM Hoechst 33342 in 3% BSA-PBS at 37°C for 15 min.

689 **Flow cytometry**

690 Flow cytometry was performed using LSRB II (Becton Dickinson). Histograms were constructed
691 using WinList 3D software (Verity Software House).

692 **ATAC-seq**

693 Two biological replicates were used for each condition. Cells were treated with 4-OHT for five
694 days and then split. After attachment, the cells were cultured in medium containing 0.5% FBS
695 for 48 hr. Cells (50,000) were prepared for ATAC-seq as previously described [35], with slight
696 modifications. Briefly, the cells were washed with PBS, lysed, and incubated with the
697 transposition reaction mixture at 37°C for 30 min. The DNA was purified using the Qiagen
698 MinElute PCR Purification Kit and amplified using PCR primer 1 and barcoded primer 2 (1 cycle
699 of 72°C for 5 min, 98°C for 30 sec, 13 cycles of 98°C for 10 sec, 63°C for 30 sec, 72°C for 1 min).
700 The primers were custom synthesized by Integrated DNA Technologies (IDT) using previously
701 described sequences [35]. The PCR products were purified using AmpureXP beads (Beckman
702 Coulter). The resulting libraries were evaluated on High-Sensitivity D1000 ScreenTape using the
703 TapeStation 4200 (Agilent Technologies). They were quantitated using the Kapa Biosystems
704 qPCR quantitation kit for Illumina. The libraries were pooled, denatured, and diluted to 350
705 pM, with a 1% PhiX control library added. The resulting pool was loaded into a NovaSeq

706 Reagent cartridge and sequenced using a NovaSeq6000 following the manufacturer's
707 recommended protocol (Illumina Inc.).

708 **RNA-seq**

709 Two biological replicates were used for each condition. Cells were treated with 4-OHT for five
710 days, then split and allowed to grow for 24 hr. The sequencing libraries were prepared from 500
711 ng total RNA using the mRNA HyperPrep kit (KAPA BIOSYSTEMS) following the manufacturer's
712 instructions. Briefly, PolyA RNA was purified using the mRNA Capture Beads. The purified RNA
713 was fragmented and primed for cDNA synthesis. Fragmented RNA was reverse transcribed into
714 first-strand cDNA using random primers. Second strand cDNA synthesis converted the
715 cDNA:RNA hybrids to double-strand cDNA (dscDNA), with the 2nd strand marked by
716 incorporating dUTP in place of dTTP. Pure Beads were used to separate the dscDNA from the
717 second-strand reaction mix, resulting in blunt-ended cDNA. A single 'A' nucleotide was added to
718 the 3' ends of the blunt fragments. Multiple indexing adapters containing a single 'T' nucleotide
719 on the 3' end were ligated to the ends of the dscDNA to prepare them for hybridization onto a
720 flow cell. The adapter-ligated libraries were amplified by PCR, purified using Pure Beads, and
721 validated for the appropriate size using a 4200 TapeStation D1000 ScreenTape (Agilent
722 Technologies, Inc.). The DNA libraries were quantitated using the KAPA Biosystems qPCR kit and
723 pooled in an equimolar fashion. Each pool was denatured and diluted to 350 pM, with a 1%
724 PhiX control library added. The resulting pools were loaded into NovaSeq Reagent cartridges for
725 100-cycle single-read analysis and sequenced with a NovaSeq6000 following the manufacturer's
726 recommended protocol (Illumina Inc.).

727 **Sample preparation for single-cell RNA-sequencing**

728 Bone marrow and intestinal cells from vehicle- and tamoxifen-treated mice were used for
729 single-cell gene expression using 10X Genomics technology. For bone marrow samples, mouse
730 femurs were cleaned with alcohol, washed with ice-cold PBS containing antibiotics, and the
731 metaphysis removed. The marrow was flushed with buffer (2 mM EDTA + 0.5% BSA in PBS)
732 using a 23G syringe. The cells were gently mixed, filtered through a 40-μm cell strainer, and
733 centrifuged at 300 g for 10 min. The pellets were resuspended in 0.04% BSA-PBS and counted
734 using trypan blue. A total of 1 x 10^5 cells were used for the analysis (1000 cells/μL).

735 For the intestinal samples, 2 cm of intestine above and below cecum, excluding cecum, were
736 excised and flushed with ice-cold PBS containing gentamycin using a 20G needle. The intestine
737 was placed in a dish with fresh PBS and cut open longitudinally. The walls were washed to
738 remove any residual matter. The intestine was incubated in ice-cold PBS containing 10 mM
739 EDTA (10 mL) at 4°C with gentle rocking for 30 min. The tissue was into ice-cold PBS and shaken
740 with vigorous bursts to release the epithelial cells. The supernatant was centrifuged at 300 g for
741 5 min at 4°C. The pellet was washed once with ice-cold PBS, resuspended in PBS containing 1
742 mg/mL collagenase, and incubated at 37°C for 5 min. The tube was then placed immediately on
743 ice, followed by the addition of 5% (v/v) FBS. The cell suspension was centrifuged, washed with
744 PBS, and filtered through a 40-μm cell strainer. The cells were resuspended in 0.04 % BSA-PBS
745 and counted using trypan blue. A total of 1 x 10^5 cells were used for the analysis (1000 cells/μL).

746 **10X Genomics**

747 Single-cell libraries were generated using the 10X Genomics platform. Cell suspensions were
748 assessed by trypan blue using the Countess FL automated cell counter (ThermoFisher) to
749 determine the concentration, viability, and absence of clumps and debris that could interfere
750 with single-cell capture. The cells were loaded into the Chromium Controller (10X Genomics),
751 where they were partitioned into nanoliter-scale Gel Beads-in-emulsion with a single barcode
752 per cell. Reverse transcription was performed, and the resulting cDNA was amplified. The full-
753 length amplified cDNA was used to generate gene expression libraries by enzymatic
754 fragmentation, end-repair, a-tailing, adapter ligation, and PCR to add Illumina-compatible
755 sequencing adapters. The resulting libraries were evaluated on D1000 ScreenTape using the
756 TapeStation 4200 (Agilent Technologies) and quantitated using the Kapa Biosystems qPCR
757 quantitation kit for Illumina. The libraries were then pooled, denatured, and diluted to 300 pM,
758 with 1% PhiX control library added. The resulting pool was loaded into the appropriate NovaSeq
759 Reagent cartridge and sequenced on a NovaSeq6000, following the manufacturer's
760 recommended protocol (Illumina Inc.).

761 **Bioinformatics analysis**

762 RNA-seq fastq files were aligned to the mouse mm10 genome using STAR [53] with GENCODE
763 v25 gene annotation. Differential gene expression was assessed using DESeq2 [54] with default
764 parameters. Genes with a 1.5-fold change between conditions and FDR < 0.05 were considered
765 differentially expressed. GSEA was run using the MSigDB website (Broad Institute), and GO
766 enrichment was run using g:Profiler [55] (Ensembl v104). The gene lists with FDR q-value ≤ 1e-4
767 were considered significant. The baseMean column from the DESeq2 differential expression

768 result table was used to classify genes based on expression levels. A list of unexpressed genes
769 was created from the genes with baseMean 0. The genes with baseMean > 0 were used for
770 ranking based on expression levels. For this ranking, the baseMean values were divided by gene
771 length and then ranked and divided into four quantiles.

772 ATAC-seq fastq files were aligned to the same genome using bowtie2 [56] with the following
773 arguments: --very-sensitive --no-mixed --no-unal --no-discordant. Duplicates were filtered using
774 the Picard MarkDuplicates function. The bigwig files with CPM-normalized profiles were
775 obtained using deepTools [57] and parameters maxFragmentlength and minFragmentlength to
776 account for the fragment sizes. Pile-ups were calculated using the computeMatrix function in
777 the scale-regions or reference-point modes and visualized using the plotProfile and
778 plotHeatmap functions from deepTools. The mean density reads at the gene bodies were
779 calculated using the ComputeMatrix function from deepTools with the following parameters:
780 scale-regions -o results.tab.gz --regionBodyLength 5000 -a 0 -b 0 --binSize 50 --
781 missingDataAsZero --skipZeros. The results.tab files for each expression category from two
782 replicates were combined into one table. Bins 21–100 were used for the calculation of the
783 mean density reads. These parameters were compared between conditions using the paired t-
784 test.

785 Single-cell RNA-seq analysis: the raw sequencing data were processed using Cellranger (version
786 5.0.0) software (10x Genomics). The filtered gene-barcode matrices, which contained the
787 barcodes with the Unique Molecular Identifier (UMI) counts that passed the cell detection
788 algorithm, were used for further analysis. The Seurat single-cell data analysis R package was

789 used for read normalization, dimension reduction, and cell clustering [58]. Cells with low RNA
790 content (detected transcripts < 200), higher mitochondrial RNA content (> 20% of total reads),
791 or very high RNA content (> 5000 detected transcripts, likely dublets) were filtered out from the
792 analysis. The mitochondrial RNA content filter was not applied for the intestine data as some of
793 the cells had very high mtRNA content, as expected [59]. Additionally, the cell cycle scores for
794 the S and G2/M phases were determined using the CellCycleScoring method based on the
795 mouse orthologous genes for the cc.genes in the Seurat package. The lists of the cell cycle
796 genes from Buettner et al [60] were used to calculate the S and G2/M scores for each cell. The
797 score was the average expression of the cell cycle genes subtracted by the aggregated
798 expression of the control feature sets, which had the same number of genes and similar
799 average gene expression value as the cell cycle genes.

800 The genes used for the S phase were Mcm4, Exo1, Slbp, Gmnn, Cdc45, Msh2, Mcm6, Rrm2,
801 Pold3, Blm, Ubr7, Mcm5, Clspn, Hells, Nasp, Rpa2, Rad51ap1, Tyms, Rrm1, Rfc2, Prim1, Brip1,
802 Usp1, Ung, Pola1, Mcm2, Fen1, Tipin, Pcna, Cdca7, Uhrf1, Casp8ap2, Cdc6, Dscc1, Wdr76, E2f8,
803 Dtl, Ccne2, Atad2, Gins2, Chaf1b, and Pcna-ps2. The G2/M genes were Nuf2, Psrc1, Ncapd2,
804 Ccnb2, Smc4, Lbr, Tacc3, Cenpa, Kif23, Cdca2, Anp32e, G2e3, Cdca3, Anln, Cenpe, Gas2l3,
805 Tubb4b, Cenpf, Dlgap5, Hjurp, Cks1brt, Gtse1, Bub1, Birc5, Ube2c, Rangap1, Hmmr, Ect2, Tpx2,
806 Ckap5, Cbx5, Nek2, Ttk, Cdca8, Nusap1, Ctcf, Cdc20, Cks2, Mki67, Tmpo, Ckap2l, Aurkb, Kif2c,
807 Cdk1, Kif20b, Top2a, Aurka, Ckap2, Hmgb2, Cdc25c, Ndc80, and Kif11.

808 The normalized and scaled UMI counts were calculated using the SCTransform method and
809 regressed against the cell cycle scores. Dimension reductions, including principal component

810 analysis (PCA) and UMAP were carried out. Data clustering was identified using shared nearest
811 neighbor (SNN)-based clustering on the first 30 principal components. Marker genes for each
812 cluster were identified using the default parameters of the FindMarkers method in the Seurat
813 package. For the bone marrow data, cell annotation was done by the singleR [61] R package
814 using the Immgen database as a reference. For the small intestine, marker genes from the
815 published single-cell data [29, 30] were used to annotate the cell types.

816 Venn diagrams were built using https://bioinformatics.psb.ugent.be/webtools/Venn/.

817 GSEA was run using MSigDB https://www.gsea-msigdb.org/gsea/msigdb/.

818 GO was run using https://biit.cs.ut.ee/gprofiler/gost.

819

820 **Statistical analyses**

821 All experiments, except scRNA sequencing, were run with at least two biological replicates and
822 included additional technical replicates (independent well, slides or fields of view). Animals
823 were randomized between groups based on genotype, gender and age. No blinding was done
824 for experiments with mice, except pathology examination of H&E stained slides. Mice
825 experiments including measurement of mouse viability and weight included groups of 5 and
826 more mice of the same gender. Other animal experiments including collection of samples for
827 different assays were done with at least 2 animals of the same gender per group. Exact number
828 of animals are provided in figure legends. Pathology examination was done without knowledge
829 of mouse genotype. Student's t-test was used to compare data between 2 groups. Details of

830 the t-test used (paired or unpaired, one or two tails distribution are provided in figure legends.
831 One-way ANOVA with Tukey posthoc tests was used to compare data between multiple groups.

832 **Acknowledgements**

833 We are grateful for the help and support of the administrative office of the Cell Stress Biology
834 Department of Roswell Park Comprehensive Cancer Center, specifically Mary Morgan, Sarah
835 Tyrpak and Bruce Specht. We thank the members of the shared resources facilities for help and
836 advice with the design and processing of the experiments, specifically Dr. Prashant Singh,
837 Director of the Genomics Shared Resource, Dr. Joseph Spernyak, Director of the Translational
838 Imaging Shared Resource, and Dr. Leslie Curtin, veterinarian in the Laboratory Animal Shared
839 Resource. We also thank Shawn Matott, a senior systems analyst, for the help with the High
840 Power Computer resources.

841 **Author contribution**

842 IG performed part of the animal experiments and most of the cell-based experiments and
843 drafted the manuscript. PS generated the mouse model, characterized the phenotypes of the
844 mice upon FACT depletion, and edited the manuscript. AS generated the genetically-modified
845 mouse embryonic stem cells and performed the *in vitro* fertilization. IT is an animal pathologist
846 who reviewed and evaluated all H&E slides. AFS performed the EU incorporation assays and
847 assisted with other experiments. MM and JW assisted with the bioinformatic analyses, and MM
848 edited the manuscript. KG developed the concept of the study, analyzed all the data, and
849 drafted and edited the manuscript.

850 **Competing interests**

851 The authors declare no competing interests related to this study.

852 **Funding**

853 This study was partially funded by a National Institutes of Health (NIH) National Cancer Institute
854 (NCI) grant to KG (R21CA198395), Roswell Park Alliance Foundation grant to KG, NCI NIH Core
855 grant to RPCCC (P30CA16056), NIH Office of Research Infrastructure Program grant to the

Center for Computational Research at the University at Buffalo (S10OD024973). The content of this article is solely the responsibility of the authors and does not necessarily represent the official views of the NIH.

Availability of data and materials

The mouse model described in this study is available from MMRRC ID:46323.

The datasets supporting the conclusions in this article are available in the GEO Datasets repository. scRNA-seq data are available as GSE189866, https://www.ncbi.nlm.nih.gov/geo/query/acc.cgi?acc=GSE189866; ATAC-seq and RNA-seq data are available as GSE189663, https://www.ncbi.nlm.nih.gov/geo/query/acc.cgi?acc=GSE189663;

The datasets supporting the conclusions of this article are included as (Tables EV1–EV4).

867 **References**

868 1. Hammond CM, Stromme CB, Huang H, Patel DJ, Groth A: **Histone chaperone networks shaping**
869 **chromatin function.** *Nat Rev Mol Cell Biol* 2017, **18:**141-158.
870 2. Dilg D, Saleh RN, Phelps SE, Rose Y, Dupays L, Murphy C, Mohun T, Anderson RH, Scambler PJ,
871 Chapgier AL: **HIRA Is Required for Heart Development and Directly Regulates Tnni2 and Tnnt3.**
872 *PLoS One* 2016, **11:**e0161096.
873 3. Shi JX, Li JS, Hu R, Li XM, Wang H: **CAF1-knockout mice are more susceptive to**
874 **lipopolysaccharide-induced acute lung injury.** *J Inflamm Res* 2016, **9:**115-121.
875 4. Messiaen S, Guiard J, Aigueperse C, Fliniaux I, Tourpin S, Barroca V, Allemand I, Fouchet P, Livera
876 G, Vernet M: **Loss of the histone chaperone ASF1B reduces female reproductive capacity in**
877 **mice.** *Reproduction* 2016, **151:**477-489.
878 5. Voon HP, Hughes JR, Rode C, De La Rosa-Velazquez IA, Jenuwein T, Feil R, Higgs DR, Gibbons RJ:
879 **ATRX Plays a Key Role in Maintaining Silencing at Interstitial Heterochromatic Loci and**
880 **Imprinted Genes.** *Cell Rep* 2015, **11:**405-418.
881 6. Formosa T, Winston F: **The role of FACT in managing chromatin: disruption, assembly, or**
882 **repair?** *Nucleic Acids Res* 2020, **48:**11929-11941.
883 7. Zhou K, Liu Y, Luger K: **Histone chaperone FACT FAcilitates Chromatin Transcription:**
884 **mechanistic and structural insights.** *Curr Opin Struct Biol* 2020, **65:**26-32.
885 8. Liu Y, Zhou K, Zhang N, Wei H, Tan YZ, Zhang Z, Carragher B, Potter CS, D'Arcy S, Luger K: **FACT**
886 **caught in the act of manipulating the nucleosome.** *Nature* 2020, **577:**426-431.
887 9. Safina A, Cheney P, Pal M, Brodsky L, Ivanov A, Kirsanov K, Lesovaya E, Naberezhnov D, Nesher
888 E, Koman I, et al: **FACT is a sensor of DNA torsional stress in eukaryotic cells.** *Nucleic Acids Res*
889 2017, **45:**1925-1945.
890 10. Tsunaka Y, Fujiwara Y, Oyama T, Hirose S, Morikawa K: **Integrated molecular mechanism**
891 **directing nucleosome reorganization by human FACT.** *Genes Dev* 2016, **30:**673-686.
892 11. Mylonas C, Tessarz P: **Transcriptional repression by FACT is linked to regulation of chromatin**
893 **accessibility at the promoter of ES cells.** *Life Science Alliance* 2018, **1:**1-14.
894 12. Sandlesh P, Safina A, Goswami I, Prendergust L, Rosario S, Gomez E, Wang J, Gurova K:
895 **Prevention of chromatin destabilization by FACT is crucial for malignant transformation**
896 *iScience* 2020.
897 13. Koltowska K, Apitz H, Stamataki D, Hirst EM, Verkade H, Salecker I, Ober EA: **Ssrp1a controls**
898 **organogenesis by promoting cell cycle progression and RNA synthesis.** *Development* 2013,
899 **140:**1912-1918.
900 14. Kolundzic E, Ofenbauer A, Bulut SI, Uyar B, Baytek G, Sommermeier A, Seelk S, He M, Hirsekorn
901 A, Vucicevic D, et al: **FACT Sets a Barrier for Cell Fate Reprogramming in Caenorhabditis**
902 **elegans and Human Cells.** *Dev Cell* 2018, **46:**611-626 e612.
903 15. Garcia H, Miecznikowski JC, Safina A, Commane M, Ruusulehto A, Kilpinen S, Leach RW, Attwood
904 K, Li Y, Degan S, et al: **Facilitates chromatin transcription complex is an "accelerator" of tumor**
905 **transformation and potential marker and target of aggressive cancers.** *Cell Rep* 2013, **4:**159-
906 173.
907 16. Fleyshman D, Prendergast L, Safina A, Paszkiewicz G, Commane M, Morgan K, Attwood K,
908 Gurova K: **Level of FACT defines the transcriptional landscape and aggressive phenotype of**
909 **breast cancer cells.** *Oncotarget* 2017, **8:**20525-20542.
910 17. Garcia H, Fleyshman D, Kolesnikova K, Safina A, Commane M, Paszkiewicz G, Omelian A,
911 Morrison C, Gurova K: **Expression of FACT in mammalian tissues suggests its role in**
912 **maintaining of undifferentiated state of cells.** *Oncotarget* 2011, **2:**783-796.

913 18. Cao S, Bendall H, Hicks GG, Nashabi A, Sakano H, Shinkai Y, Gariglio M, Oltz EM, Ruley HE: **The**
914 **high-mobility-group box protein SSRP1/T160 is essential for cell viability in day 3.5 mouse**
915 **embryos.** *Mol Cell Biol* 2003, **23:**5301-5307.
916 19. Safina A, Garcia H, Commane M, Guryanova O, Degan S, Kolesnikova K, Gurova KV: **Complex**
917 **mutual regulation of facilitates chromatin transcription (FACT) subunits on both mRNA and**
918 **protein levels in human cells.** *Cell Cycle* 2013, **12:**2423-2434.
919 20. Sandlesh P, Juang T, Safina A, Higgins MJ, Gurova KV: **Uncovering the fine print of the CreERT2-**
920 **LoxP system while generating a conditional knockout mouse model of Ssrp1 gene.** *PLoS One*
921 2018, **13:**e0199785.
922 21. Luo S, Martel C, Sourla A, Gauthier S, Merand Y, Belanger A, Labrie C, Labrie F: **Comparative**
923 **effects of 28-day treatment with the new anti-estrogen EM-800 and tamoxifen on estrogen-**
924 **sensitive parameters in intact mice.** *Int J Cancer* 1997, **73:**381-391.
925 22. Su L, Mruk DD, Cheng CY: **Drug transporters, the blood-testis barrier, and spermatogenesis.** *J*
926 *Endocrinol* 2011, **208:**207-223.
927 23. Abe T, Sugimura K, Hosono Y, Takami Y, Akita M, Yoshimura A, Tada S, Nakayama T, Murofushi
928 H, Okumura K, et al: **The histone chaperone facilitates chromatin transcription (FACT) protein**
929 **maintains normal replication fork rates.** *J Biol Chem* 2011, **286:**30504-30512.
930 24. Prendergast L, Hong E, Safina A, Poe D, K. G: **Histone chaperone FACT is essential to overcome**
931 **replication stress in mammalian cells.** *Oncogene* 2020, **under revision**
932 25. Tan BC, Chien CT, Hirose S, Lee SC: **Functional cooperation between FACT and MCM helicase**
933 **facilitates initiation of chromatin DNA replication.** *EMBO J* 2006, **25:**3975-3985.
934 26. Yang J, Zhang X, Feng J, Leng H, Li S, Xiao J, Liu S, Xu Z, Xu J, Li D, et al: **The Histone Chaperone**
935 **FACT Contributes to DNA Replication-Coupled Nucleosome Assembly.** *Cell Rep* 2016, **14:**1128-
936 1141.
937 27. Zeng SX, Li Y, Jin Y, Zhang Q, Keller DM, McQuaw CM, Barklis E, Stone S, Hoatlin M, Zhao Y, Lu H:
938 **Structure-specific recognition protein 1 facilitates microtubule growth and bundling required**
939 **for mitosis.** *Mol Cell Biol* 2010, **30:**935-947.
940 28. Immunological Genome P: **ImmGen at 15.** *Nat Immunol* 2020, **21:**700-703.
941 29. Gao S, Yan L, Wang R, Li J, Yong J, Zhou X, Wei Y, Wu X, Wang X, Fan X, et al: **Tracing the**
942 **temporal-spatial transcriptome landscapes of the human fetal digestive tract using single-cell**
943 **RNA-sequencing.** *Nat Cell Biol* 2018, **20:**721-734.
944 30. Haber AL, Biton M, Rogel N, Herbst RH, Shekhar K, Smillie C, Burgin G, Delorey TM, Howitt MR,
945 Katz Y, et al: **A single-cell survey of the small intestinal epithelium.** *Nature* 2017, **551:**333-339.
946 31. Lindeboom RG, van Voorthuijsen L, Oost KC, Rodriguez-Colman MJ, Luna-Velez MV, Furlan C,
947 Baraille F, Jansen PW, Ribeiro A, Burgering BM, et al: **Integrative multi-omics analysis of**
948 **intestinal organoid differentiation.** *Mol Syst Biol* 2018, **14:**e8227.
949 32. Wittenburg G, Flade V, Garbe AI, Lauer G, Labudde D: **Scaffold preferences of mesenchymal**
950 **stromal cells and adipose-derived stem cells from green fluorescent protein transgenic mice**
951 **influence the tissue engineering of bone.** *Br J Oral Maxillofac Surg* 2014, **52:**409-414.
952 33. Taha MF, Hedayati V: **Isolation, identification and multipotential differentiation of mouse**
953 **adipose tissue-derived stem cells.** *Tissue Cell* 2010, **42:**211-216.
954 34. Huang SJ, Fu RH, Shyu WC, Liu SP, Jong GP, Chiu YW, Wu HS, Tsou YA, Cheng CW, Lin SZ:
955 **Adipose-derived stem cells: isolation, characterization, and differentiation potential.** *Cell*
956 *Transplant* 2013, **22:**701-709.
957 35. Buenrostro JD, Giresi PG, Zaba LC, Chang HY, Greenleaf WJ: **Transposition of native chromatin**
958 **for fast and sensitive epigenomic profiling of open chromatin, DNA-binding proteins and**
959 **nucleosome position.** *Nat Methods* 2013, **10:**1213-1218.

960 36. Suto RK, Edayathumangalam RS, White CL, Melander C, Gottesfeld JM, Dervan PB, Luger K:
961 **Crystal structures of nucleosome core particles in complex with minor groove DNA-binding**
962 **ligands.** *J Mol Biol* 2003, **326:**371-380.
963 37. Fitzgerald DJ, Anderson JN: **Selective nucleosome disruption by drugs that bind in the minor**
964 **groove of DNA.** *J Biol Chem* 1999, **274:**27128-27138.
965 38. Orphanides G, LeRoy G, Chang CH, Luse DS, Reinberg D: **FACT, a factor that facilitates transcript**
966 **elongation through nucleosomes.** *Cell* 1998, **92:**105-116.
967 39. Formosa T, Winston F: **The role of FACT in managing chromatin: disruption, assembly, or**
968 **repair?** *Nucleic Acids Res* 2020, **48:**11929-11941.
969 40. Gurova K, Chang HW, Valieva ME, Sandlesh P, Studitsky VM: **Structure and function of the**
970 **histone chaperone FACT - Resolving FACTual issues.** *Biochim Biophys Acta Gene Regul Mech*
971 2018.
972 41. Carvalho S, Raposo AC, Martins FB, Grosso AR, Sridhara SC, Rino J, Carmo-Fonseca M, de
973 Almeida SF: **Histone methyltransferase SETD2 coordinates FACT recruitment with nucleosome**
974 **dynamics during transcription.** *Nucleic Acids Res* 2013, **41:**2881-2893.
975 42. Mason PB, Struhl K: **The FACT complex travels with elongating RNA polymerase II and is**
976 **important for the fidelity of transcriptional initiation in vivo.** *Mol Cell Biol* 2003, **23:**8323-8333.
977 43. True JD, Muldoon JJ, Carver MN, Poorey K, Shetty SJ, Bekiranov S, Auble DT: **The Modifier of**
978 **Transcription 1 (Mot1) ATPase and Spt16 Histone Chaperone Co-regulate Transcription**
979 **through Preinitiation Complex Assembly and Nucleosome Organization.** *J Biol Chem* 2016,
980 **291:**15307-15319.
981 44. Nesher E, Safina A, Aljahdali I, Portwood S, Wang ES, Koman I, Wang J, Gurova KV: **Role of**
982 **chromatin damage and chromatin trapping of FACT in mediating the anticancer cytotoxicity of**
983 **DNA-binding small molecule drugs.** *Cancer Res* 2018.
984 45. Hsieh FK, Kulaeva OI, Patel SS, Dyer PN, Luger K, Reinberg D, Studitsky VM: **Histone chaperone**
985 **FACT action during transcription through chromatin by RNA polymerase II.** *Proc Natl Acad Sci U*
986 *S A* 2013, **110:**7654-7659.
987 46. Li W, Chen P, Yu J, Dong L, Liang D, Feng J, Yan J, Wang PY, Li Q, Zhang Z, et al: **FACT Remodels**
988 **the Tetranucleosomal Unit of Chromatin Fibers for Gene Transcription.** *Mol Cell* 2016, **64:**120-
989 133.
990 47. Stetson DB, Medzhitov R: **Type I interferons in host defense.** *Immunity* 2006, **25:**373-381.
991 48. Leonova K, Safina A, Nesher E, Sandlesh P, Pratt R, Burkhart C, Lipchick B, Gitlin I, Frangou C,
992 Koman I, et al: **TRAIN (Transcription of Repeats Activates INterferon) in response to chromatin**
993 **destabilization induced by small molecules in mammalian cells.** *Elife* 2018, **7**.
994 49. Unterholzner L: **The interferon response to intracellular DNA: why so many receptors?**
995 *Immunobiology* 2013, **218:**1312-1321.
996 50. Michalski S, de Oliveira Mann CC, Stafford CA, Witte G, Bartho J, Lammens K, Hornung V,
997 Hopfner KP: **Structural basis for sequestration and autoinhibition of cGAS by chromatin.**
998 *Nature* 2020, **587:**678-682.
999 51. Parasuraman S, Raveendran R, Kesavan R: **Blood sample collection in small laboratory animals.**
1000 *J Pharmacol Pharmacother* 2010, **1:**87-93.
1001 52. Sato T, Vries RG, Snippert HJ, van de Wetering M, Barker N, Stange DE, van Es JH, Abo A, Kujala
1002 P, Peters PJ, Clevers H: **Single Lgr5 stem cells build crypt-villus structures in vitro without a**
1003 **mesenchymal niche.** *Nature* 2009, **459:**262-265.
1004 53. Dobin A, Davis CA, Schlesinger F, Drenkow J, Zaleski C, Jha S, Batut P, Chaisson M, Gingeras TR:
1005 **STAR: ultrafast universal RNA-seq aligner.** *Bioinformatics* 2013, **29:**15-21.
1006 54. Love MI, Huber W, Anders S: **Moderated estimation of fold change and dispersion for RNA-seq**
1007 **data with DESeq2.** *Genome Biol* 2014, **15:**550.

1008 55. Raudvere U, Kolberg L, Kuzmin I, Arak T, Adler P, Peterson H, Vilo J: **g:Profiler: a web server for**
1009 **functional enrichment analysis and conversions of gene lists (2019 update).** *Nucleic Acids Res*
1010 2019, **47:**W191-W198.
1011 56. Langmead B, Salzberg SL: **Fast gapped-read alignment with Bowtie 2.** *Nat Methods* 2012, **9:**357-
1012 359.
1013 57. Ramirez F, Dundar F, Diehl S, Gruning BA, Manke T: **deepTools: a flexible platform for exploring**
1014 **deep-sequencing data.** *Nucleic Acids Res* 2014, **42:**W187-191.
1015 58. Satija R, Farrell JA, Gennert D, Schier AF, Regev A: **Spatial reconstruction of single-cell gene**
1016 **expression data.** *Nat Biotechnol* 2015, **33:**495-502.
1017 59. Osorio D, Cai JJ: **Systematic determination of the mitochondrial proportion in human and mice**
1018 **tissues for single-cell RNA-sequencing data quality control.** *Bioinformatics* 2021, **37:**963-967.
1019 60. Buettner F, Natarajan KN, Casale FP, Proserpio V, Scialdone A, Theis FJ, Teichmann SA, Marioni
1020 JC, Stegle O: **Computational analysis of cell-to-cell heterogeneity in single-cell RNA-sequencing**
1021 **data reveals hidden subpopulations of cells.** *Nat Biotechnol* 2015, **33:**155-160.
1022 61. Aran D, Looney AP, Liu L, Wu E, Fong V, Hsu A, Chak S, Naikawadi RP, Wolters PJ, Abate AR, et al:
1023 **Reference-based analysis of lung single-cell sequencing reveals a transitional profibrotic**
1024 **macrophage.** *Nat Immunol* 2019, **20:**163-172.

1025

1026

Figure Legends

Figure 1. Effect of *Ssrp1* KO in adult mice.

A, B. Normalized weight (A) and survival (B) of *Ssrp1*$^{fl/fl}$*; CreER*$^{T2+/+}$ mice of different ages (weeks) after the start of tamoxifen (TMX) treatment. A. Mean weight (%) ± SD. P < 0.05 for all tamoxifen treated groups versus vehicle (ANOVA). B. Kaplan-Meier survival curves. Log-rank test p = 0.032 for the oldest male age group versus all other male groups; p = 0.013 for all females versus all males; for all other comparisons p > 0.05. *n = 6-10 mice*.

C. Normalized blood cell counts in *Ssrp1*$^{fl/fl}$*; CreER*$^{T2+/+}$ mice treated with vehicle or tamoxifen on day 7 after start of treatment. Mean ± SD, * indicates p < 0.05 (unpaired t-test). *n = 3 mice*.

D. Photographs of vehicle- or tamoxifen-treated *Ssrp1*$^{fl/fl}$*; CreER*$^{T2+/+}$ mice seven days after start of treatment.

E. Gross pathology examination of *Ssrp1*$^{fl/fl}$*; CreER*$^{T2+/+}$ mouse euthanized due to 20% weight loss after treatment with tamoxifen. Vehicle-treated mouse is shown for comparison. Green and blue ovals indicate subcutaneous and inguinal fat deposits, respectively.

F. MRI image of *Ssrp1*$^{fl/fl}$*; CreER*$^{T2+/+}$ mouse before and after tamoxifen treatment.

Figure 2. Pathological findings in *Ssrp1*$^{fl/fl}$*; CreER*$^{T2+/+}$ mice after tamoxifen treatment.

A. H&E staining of mouse organ sections. Scale bars: spleen, colon 100 μM, bone marrow – 50 μM.

B. Incidence of pathological findings (number of mice with pathology/total number of mice).

C. H&E staining of liver sections. Yellow arrow - a mitotic hepatocyte; blue arrows - lymphocyte infiltration. Scale bars – 100 μM.

Figure 3. FACT depletion in mice leads to reduced proliferation and cells death in several organs.

A, B. Effect of tamoxifen on replication in the spleen (A) and intestine (B) of *Ssrp1*$^{fl/fl}$*; CreER*$^{T2+/+}$ mice. EdU was given to mice three days after the end of tamoxifen treatment

(1 hour before tissue collection). Organ sections were stained for total DNA (Hoechst), EdU, and SSRP1. Scale bars – 100 μM.

C. Quantitation of EdU staining. Mean number of EdU positive cells per field of view +/- SD. *n* $\geq$ *5 fields of view*. 3 mice were analyzed.

D. Quantitation of cleaved caspase-3 staining. Mean number of positive cells per fields of view +/- SD, *n* $\geq$ *5 fields of view.* Two male and female mice were analyzed.

P-values for C and D were calculated using the unpaired t-test.

Figure 4. Effect of FACT depletion on cell composition of bone marrow from *Ssrp1*$^{fl/fl}$*; CreER*$^{T2+/+}$ mice (pooled data from two mice on day 1 after the end of treatment).

A. UMAP plots with unbiasedly identified clusters shown in different colors.

B. UMAP plots colored according to cell type identified by transcriptional signatures using the Immgen database as a reference.

C. Distribution of bone marrow cell types in vehicle- and tamoxifen-treated mice. The pie charts are colored accordingly to panel B. Only cell types with more than ten cells in any of the conditions are included.

D. Fold-change in the proportion of cells in each cluster shown in panel A in samples from tamoxifen-treated versus vehicle-treated mice. Cell types are identified by color as in panel B.

E. Distribution of different types of bone marrow stem cells from vehicle- and tamoxifen-treated mice. Stem cell types were identified by transcriptional signatures using the Immgen stem cell database as a reference. Only cell types with more than five cells in any of the conditions identified are presented. LTHSC – long-term hematopoietic stem cells (HSC), ST34F – CD34+Flk2- short-term (ST) HSC, STSL – ST reconstituting stem cells, MPP34F – CD34+Flk2+ multipotent progenitors, MLP – multi-lymphoid progenitors, CMP.DR – common myeloid progenitor, MEP – megakaryocyte-erythroid progenitors, MDP – monocyte-dendritic cell progenitors, CDP – common dendritic cell progenitors, GMP – granulocyte-monocyte progenitor.

F. Changes in the abundance and distribution of major bone marrow stem cell types. Center – UMAP plots showing enlarged regions as colored dashed rectangles. The color of a rectangle corresponds to the color of the stem cells in individual sections. Around central UMAPs – enlarged sections of the central UMAP plot showing individual stem cell subtypes. Colored dots – corresponding stem cells, grey dots – other cells.

G–H. GSEA of gene markers of neutrophil (G) or B cell (H) in clusters enlarged upon FACT loss (red) or reduced upon FACT loss (blue).

Figure 5. Effect of FACT depletion on cell composition of the intestine from *Ssrp1*$^{fl/fl}$*; CreER*$^{T2+/+}$ mice (pooled data from two mice on day 1 after the end of treatment).

A. UMAP plots with unbiasedly identified clusters shown in different colors.

B. UMAP plots are colored according to cell type identified by transcriptional signatures using data from [29] as a reference. LI – large intestine, SI – small intestine.

C. Distribution of intestinal cell types in samples from vehicle- and tamoxifen-treated mice. Pie charts are colored accordingly to panel B.

D. UMAP plots with color-coded intestinal stem cells identified by transcriptional signatures of intestinal stem cells from [30] or by expression of *Lgr5* or *Gkn3* genes.

E. UMAP plots showing the distribution of cells with transcriptional signatures of proximal and distal enterocytes from [30] and cells expressing the *Dclk1* gene.

F. GSEA of gene markers of clusters 2 and 3 (lost upon *Ssrp1* KO, blue) versus clusters 8 and 9 (emerged upon *Ssrp1* KO, red).

Figure 6. FACT depletion affects the viability of stem cells but not differentiated cells.

A, B. Effect of 4-OHT administration on colony formation by bone marrow cells of different genotypes*. A.* Photographs of colonies from bone marrow cells kept in culture for seven days in the presence or absence of 4-OHT. B. Quantitation of bone marrow colony assay. Mean colony number per plate ± SD, *n = 3 plates*. P values < 0.05 are shown (unpaired t-test). 2 mice of each genotype were analyzed.

C, D. Growth of intestinal organoids in the presence or absence of 4-OHT. C. Photographs of small intestine organoids on different days after plating. D. Number of organoids in the presence and absence of 4-OHT. Mean fold change between number of organoids in control and 4-OHT treated wells ± SD, *n = 4 wells*. P < 0.05 are shown (unpaired t-test). Organoids were isolated from one mouse of each genotype in two independent experiments.

E. Caspase activity in lysates of control and 4-OHT treated MSCs of different genotypes. Mean fold change ± SD, *n = 3 plates*. P < 0.05 are shown (unpaired t-test). MSCs were isolated from 2-3 mice of each genotype.

F, G. Effect of 4-OHT administration on intestinal organoids of different genotypes kept in the presence (undifferentiated) or absence (differentiated) of R-spondin-1. F. The viability of organoids assessed by the resorufin assay. Mean ± SD, *n = 3 wells*. P < 0.05 are shown (unpaired t-test). Organoids were isolated from two mice of each genotype. G. IF images of intestinal organoids from *Ssrp1*$^{fl/fl}$*; CreER*$^{T2+/+}$ mice kept in the presence or absence of R-Spondin-1. The organoids were stained with antibodies to LGR5 and SSRP1 and counterstained with Hoechst (DNA).

H–J. Effect of 4-OHT administration on MSCs and their differentiated counterparts. H. Methylene blue viability assay for undifferentiated MSCs or MSCs differentiated into osteocytes or adipocytes for 21 days and then treated with vehicle or 4-OHT. Mean ± SD, n = 3 plates. P < 0.05 are shown (unpaired t-test). MSCs were isolated from two mice of each genotype. H. Staining of MSCs, osteocytes, and adipocytes with Alizarine Red (osteocytes) or Oil Red (adipocytes). J. Western blotting of protein extracts from MSCs, adipocytes, and osteocytes from mice of different genotypes treated with vehicle or 4-OHT.

Figure 7. Comparison of transcription between *Ssrp1*$^{fl/fl}$*; CreER*$^{T2+/+}$ MSCs treated with vehicle or 4-OHT.

A. EU incorporation measured by flow cytometry. Histograms of EU fluorescent signals from two replicates for each condition (except no EU).

B. SSRP1 staining of the cells in A.

C. Volcano plot of changes in transcript counts in 4-OHT-treated cells versus control. Red dots indicate transcripts with fold-change $\geq$ 2 and FDR < 0.05. *n = 2 cell cultures*.

B. MA plot showing the difference between the changes in transcript counts in 4-OHT-treated MSCs vs. control and the average expression of the same transcripts between conditions (baseMean). *n = 2 cell cultures*.

C, D. Dot plots with the results of GO enrichment for genes upregulated (C) and downregulated (D) upon FACT depletion.

Figure 8. FACT depletion in *Ssrp1*$^{fl/fl}$*; CreER*$^{T2+/+}$ MSCs leads to increase in chromatin accessibility in a transcription-dependent manner.

A–B. Profiles and heatmaps for normalized ATAC-seq read distribution averaged for all known mouse genes in control or 4-OHT-treated MSCs for reads below 120 bp (A,

nucleosome-free) and between 120 and 250 bp (B, mononucleosomes). One of two replicates is shown.

C–D. ATAC-seq read density profile for two replicates of control and treated MSCs for all mouse genes of the nucleosome-free (C) and mononucleosome (D) fragments.

E–F. ATAC-seq read density profiles for nucleosome-free (E) and mononucleosome (F) fragments for differentially expressed genes.

G. Box plots of mean read density at the gene body (bins 21–100 out of 100 between TSS – TES) for all genes and differentially expressed genes. *** - $p < 1e-10$ (paired t-test). *n = 2 cell cultures*.

H. Comparison of Hoechst 33342 binding to live control and 4-OHT-treated MSCs from different genotypes. Data are presented as the median fluorescence intensity ± SD, *n = 4 cell cultures*. $P < 0.05$ is shown (unpaired t-test).

Expanded View Figure Legends

Figure EV1.

A. Kinetic of FACT protein subunit loss in spleen of *Ssrp1*$^{fl/fl}$*; CreER*$^{T2+/+}$ mice upon tamoxifen administration. Western blotting of total protein extracts of spleen collected from mice at indicated time points. Veh is vehicle. B. Kinetic of weight changes of *Ssrp1*$^{+/+}$ *; CreER*$^{T2+/+}$ mice upon tamoxifen administration. Mean +/- SD. C. Effect of rehydration on weight of *Ssrp1*$^{+/+}$ *; CreER*$^{T2+/+}$ mice treated with vehicle or tamoxifen. Kinetic of weight loss in control and tamoxifen treated animals either provided with subcutaneous saline injection (1 or 2 ml per day) or not. Mean +/- SD, n = 3. D. Effect of rehydration on survival of *Ssrp1*$^{+/+}$ *; CreER*$^{T2+/+}$ mice treated with vehicle or tamoxifen. Kaplan-Mayer curves of control and tamoxifen treated groups either provided with subcutaneous saline injection (1 or 2 ml per day) or not. n = 3. E. Changes in organ weight in *Ssrp1*$^{fl/fl}$*; CreER*$^{T2+/+}$ mice treated with tamoxifen versus vehicle treated animals. Mean +/- SD. * - p-value <0.05. n = 5. F – G. Representative photographs of female (F) and male (G) reproductive organs excised from vehicle and tamoxifen treated mice.

Figure EV2.

A-B. Effect of tamoxifen administration to *Ssrp1*$^{fl/fl}$*; CreER*$^{T2+/+}$ mice on replication in testis (A) and liver (B). EdU was given to mice 3 days after stop of tamoxifen treatment for 1 hour followed by organ isolation and staining for total DNA (Hoechst), EdU and SSRP1. Red arrow indicates EdU positive nucleus in liver. C. Staining of sections of several organs of in *Ssrp1*$^{fl/fl}$*; CreER*$^{T2+/+}$ mice for cleaved caspase 3 three days after stop of treatment with tamoxifen or vehicle.

Figure EV3.

Analyses of scRNA sequencing of bone marrow and intestine of in *Ssrp1*$^{fl/fl}$*; CreER*$^{T2+/+}$ mice next day after stop of treatment with vehicle or tamoxifen. A. Comparison of the numbers of sequenced cells, mean reads per cell and mean identified genes between samples. B. Dot plots showing the number of features (nFeature_RNA, the number of genes detected in each cell), RNA molecules (nCount_RNA, he total number of molecules detected within a cell) and proportion of reads corresponding to mitochondrial RNA (percent.mito) in each sample. C. Overlapped UMAP plots of bone marrow and intestinal samples color coded according to the treatment type. D-E. UMAP plots of bone marrow (D) and intestine (E) color-coded based on the expression of markers of cell cycle.

Figure EV4.

Comparison of changes in transcription in MSC of two genotypes treated with vehicle of 4-OHT for 5 days and then split and analyzed 24 hour after. A-B. EU incorporation assay (30 min) (A) and staining with SSRP1 antibody (B) of *Ssrp1*$^{fl/+}$*; CreER*$^{T2+/+}$ MSC. Two replicates are shown. C - E. Data of RNA-seq experiment with two replicates of MSC. C. Venn diagrams showing number of up- and downregulated genes in homo- and heterozygous cells. D. Volcano plot of gene

1207 expression changes in heterozygous cells upon 4-OHT treatment. E. MA plot of gene expression
1208 changes in heterozygous cells upon 4-OHT treatment.

1209

1210 **Figure EV5.**

1211 Assessment of general chromatin accessibility by staining DNA in live cells with Hoechst 33342.
1212 Histograms of fluorescent intensity of MSC stained with 3uM of Hoechst 33342 for 15 min. A.
1213 After incubation with CBL0137 (1uM) for 30 min. This plot also includes overlap of histogram of
1214 negative control (cells unstained with Hoechst). B. *Ssrp1*$^{fl/fl}$*; CreER*$^{T2+/+}$ cells untreated or treated
1215 with 4OHT. C. *Ssrp1*$^{fl/+}$*; CreER*$^{T2+/-}$ cells untreated or treated with 4OHT.

1216

1217

1218

1219

1220

1221

1222

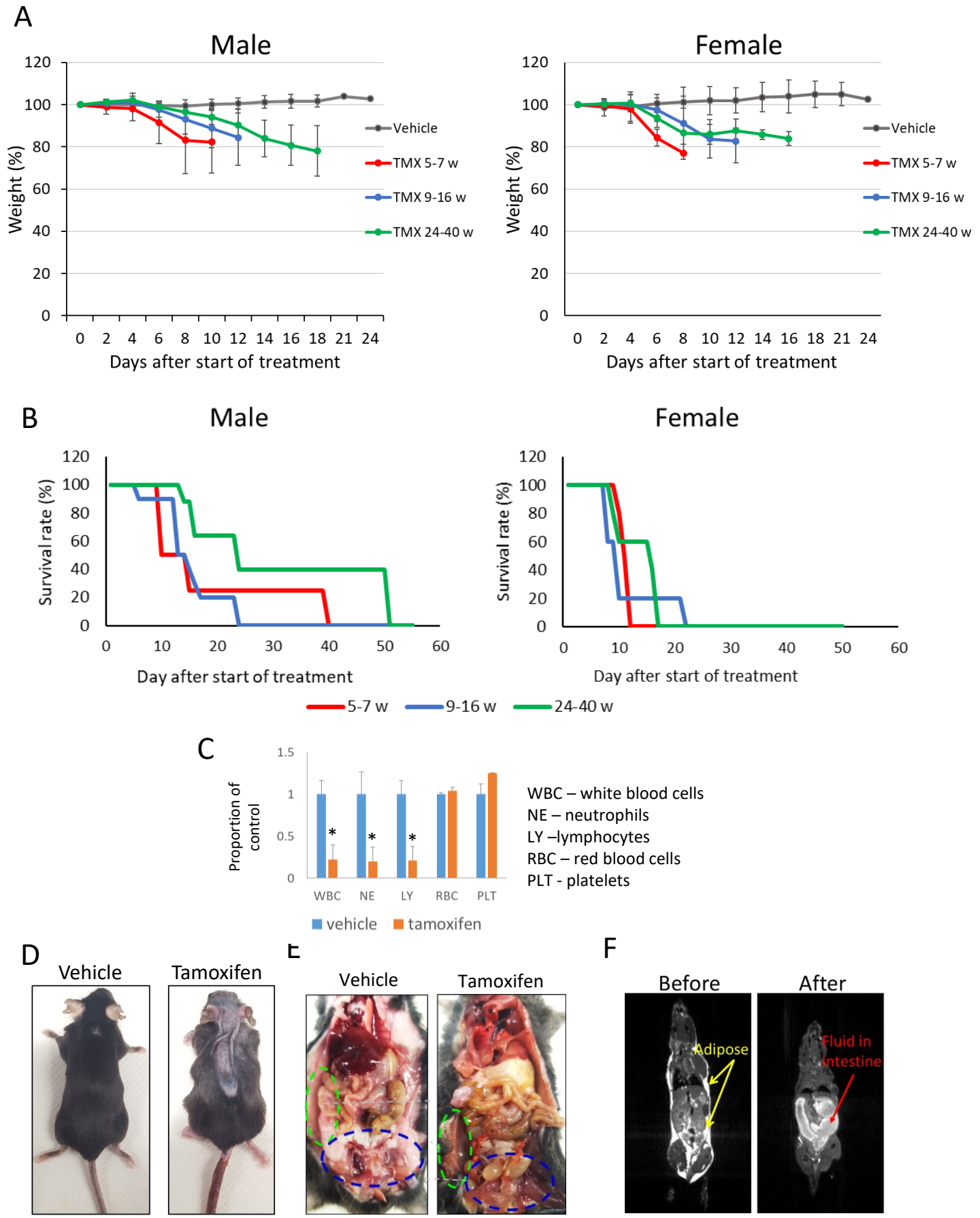
A
Male
Female
Weight (%)
Days after start of treatment
Vehicle
TMX 5-7 w
TMX 9-16 w
TMX 24-40 w
B
Survival rate (%)
Day after start of treatment
5-7 w
9-16 w
24-40 w
C
Proportion of control
WBC
NE
LY
RBC
PLT
vehicle
tamoxifen
WBC – white blood cells
NE – neutrophils
LY –lymphocytes
RBC – red blood cells
PLT - platelets
D
Vehicle
Tamoxifen
E
Vehicle
Tamoxifen
F
Before
After
Adipose
Fluid in intestine

Figure 1

A

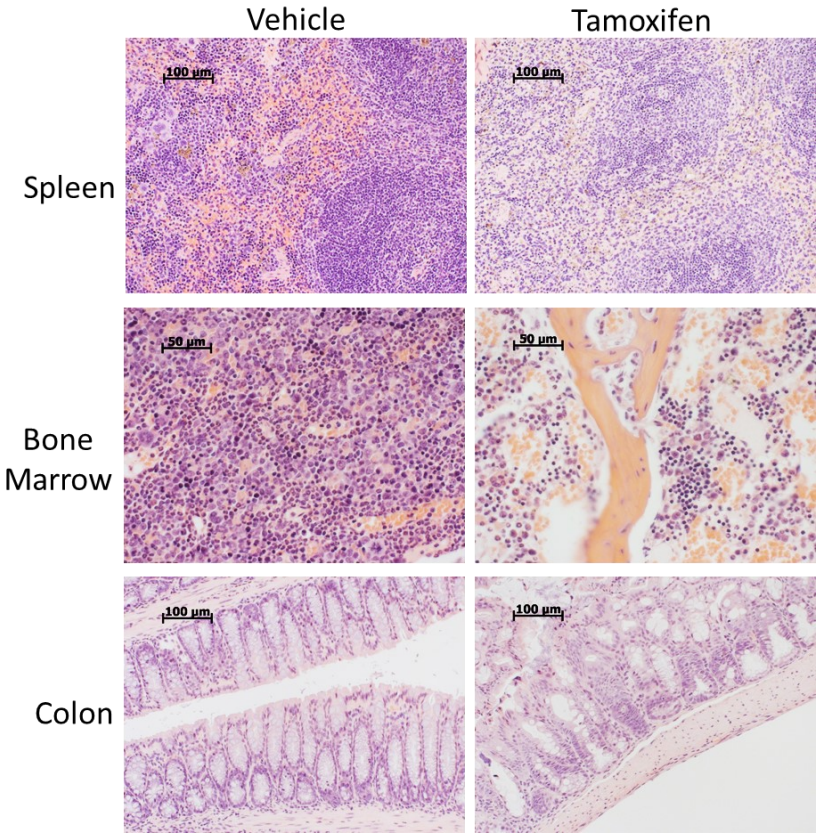

B

Organs	Vehicle		Tamoxifen	
	M (n=4)	F (n=2)	M (n=5)	F (n=4)
Liver	1/4	0/2	5/5	4/4
Lung	0/4	0/2	0/5	0/4
Bone Marrow	0/4	0/2	3/5	3/4
Spleen	0/4	0/2	2/5	3/4
Colon	0/4	0/2	2/5	2/5
Duodenum	0/4	0/2	1/5	1/4
Skin	0/4	0/2	4/5	0/4
Salivary Gland	0/4	0/2	3/5	0/4
Pancreas	0/4	0/2	2/5	0/4
Kidney	0/4	0/2	0/5	3/5

C

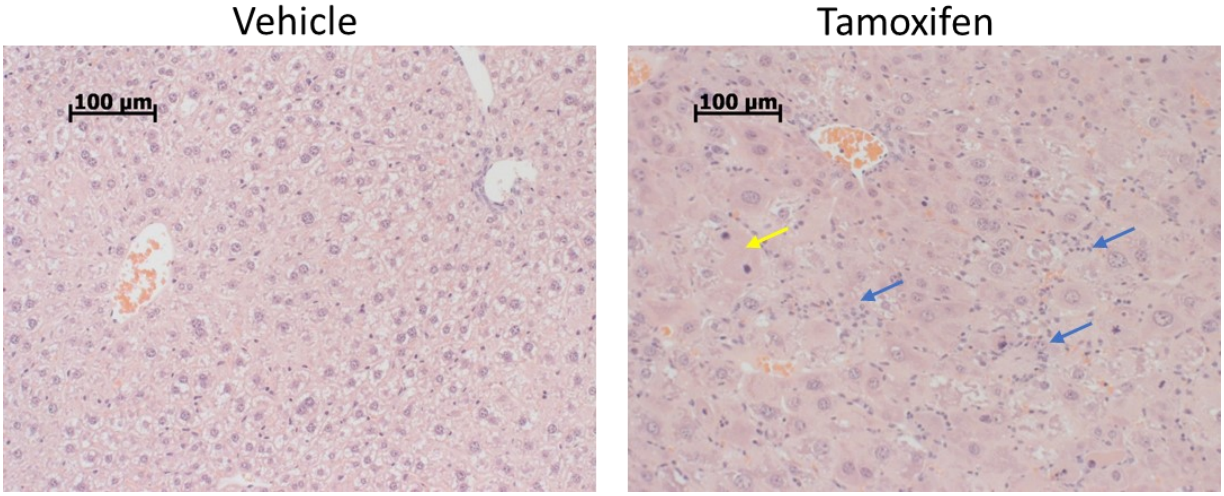

Figure 2

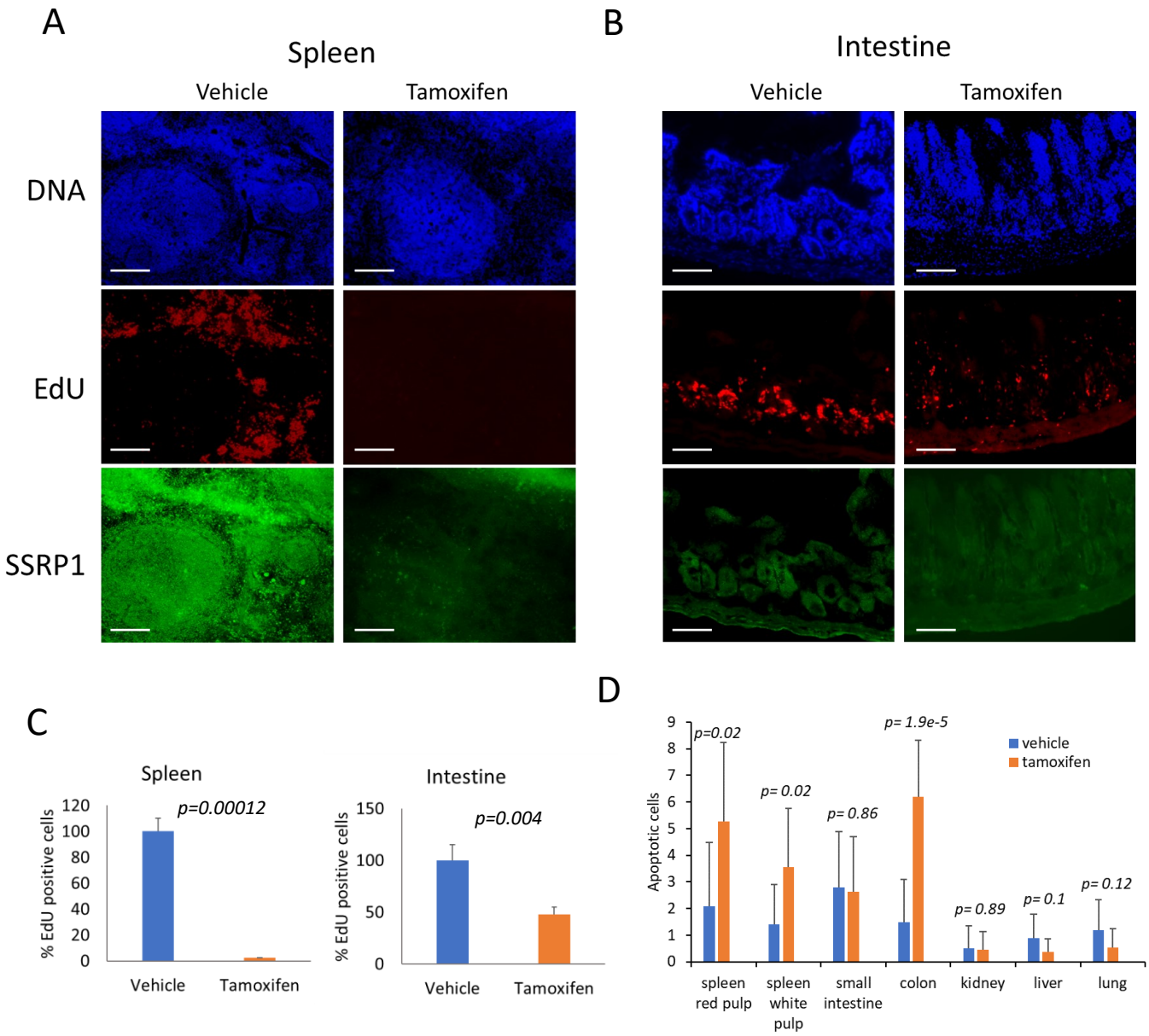
A
Spleen
Vehicle
Tamoxifen
DNA
EdU
SSRP1
B
Intestine
Vehicle
Tamoxifen
C
Spleen
% EdU positive cells
120
100
80
60
40
20
0
p=0.00012
Vehicle
Tamoxifen
Intestine
% EdU positive cells
150
100
50
0
p=0.004
Vehicle
Tamoxifen
D
Apoptotic cells
9
8
7
6
5
4
3
2
1
0
p=0.02
p= 0.02
p= 0.86
p= 1.9e-5
p= 0.89
p= 0.1
p= 0.12
vehicle
tamoxifen
spleen red pulp
spleen white pulp
small intestine
colon
kidney
liver
lung

Figure 3

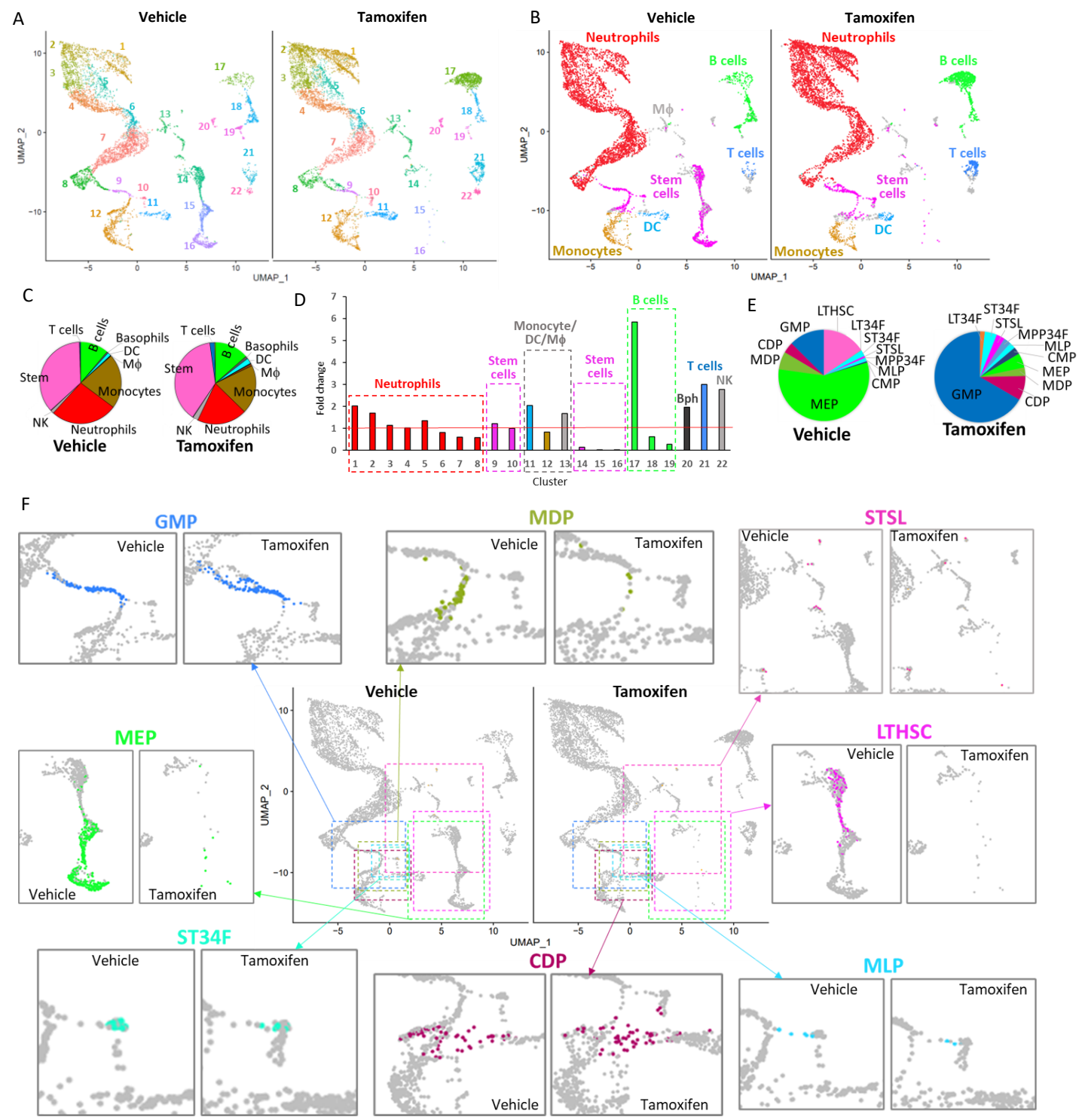
A
Vehicle
Tamoxifen
UMAP_1
UMAP_2
B
Neutrophils
B cells
Mϕ
T cells
Stem cells
DC
Monocytes
C
T cells
B cells
Basophils
DC
Mϕ
Stem
Monocytes
NK
Neutrophils
Vehicle
Tamoxifen
D
Fold change
Neutrophils
Stem cells
Monocyte/ DC/Mϕ
Stem cells
B cells
T cells
Bph
NK
Cluster
E
LTHSC
GMP
LT34F
ST34F
STSL
CDP
MDP
MPP34F
MLP
CMP
MEP
Vehicle
Tamoxifen
F
GMP
MDP
STSL
MEP
LTHSC
ST34F
CDP
MLP
Vehicle
Tamoxifen
G
Clusters
6, 7, 8
1, 2, 3, 5
Cell cycle targets of E2F
G2/M checkpoint
MYC targets
Mitotic spindle assembly
Glycolysis and gluconeogenesis
Upregulated via mTORC1
IFNγ response
NF-κB response to TNF
Upregulated by IL6 via STAT3
IFNα response
Apoptosis genes
p53 pathways
-Log10(FDR)
H
Clusters
17
18, 19
MYC targets
G2M checkpoint
E2F targets
IFNγ response
Unfolded protein response
Allograft rejection
IFNγ response
Complement
-Log10(FDR)

Figure 4

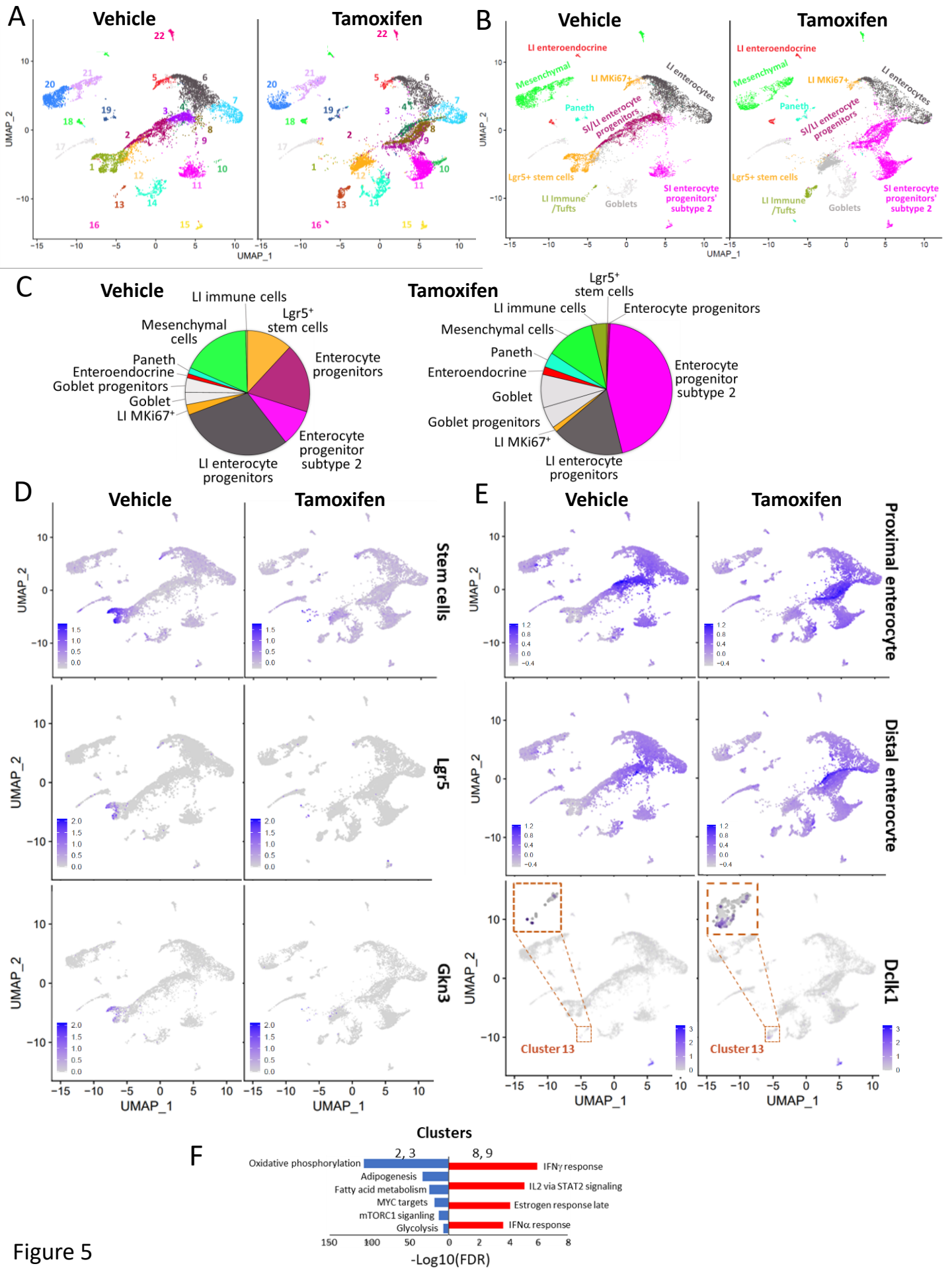
A
Vehicle
Tamoxifen
UMAP_1
UMAP_2
B
Vehicle
Tamoxifen
LI enteroendocrine
Mesenchymal
LI MKi67+
LI enterocytes
Paneth
SI/LI enterocyte progenitors
Lgr5+ stem cells
LI Immune /Tufts
Goblets
SI enterocyte progenitors' subtype 2
C
Vehicle
LI immune cells
Lgr5+ stem cells
Mesenchymal cells
Enterocyte progenitors
Paneth
Enteroendocrine
Goblet progenitors
Goblet
LI MKi67+
Enterocyte progenitor subtype 2
LI enterocyte progenitors
Tamoxifen
Lgr5+ stem cells
LI immune cells
Enterocyte progenitors
Mesenchymal cells
Paneth
Enteroendocrine
Goblet
Goblet progenitors
LI MKi67+
Enterocyte progenitor subtype 2
LI enterocyte progenitors
D
Vehicle
Tamoxifen
Stem cells
Lgr5
Gkn3
E
Vehicle
Tamoxifen
Proximal enterocyte
Distal enterocyte
Dclk1
Cluster 13
Cluster 13
F
Clusters
2, 3
8, 9
Oxidative phosphorylation
Adipogenesis
Fatty acid metabolism
MYC targets
mTORC1 siganling
Glycolysis
IFNγ response
IL2 via STAT2 signaling
Estrogen response late
IFNα response
-Log10(FDR)

Figure 5

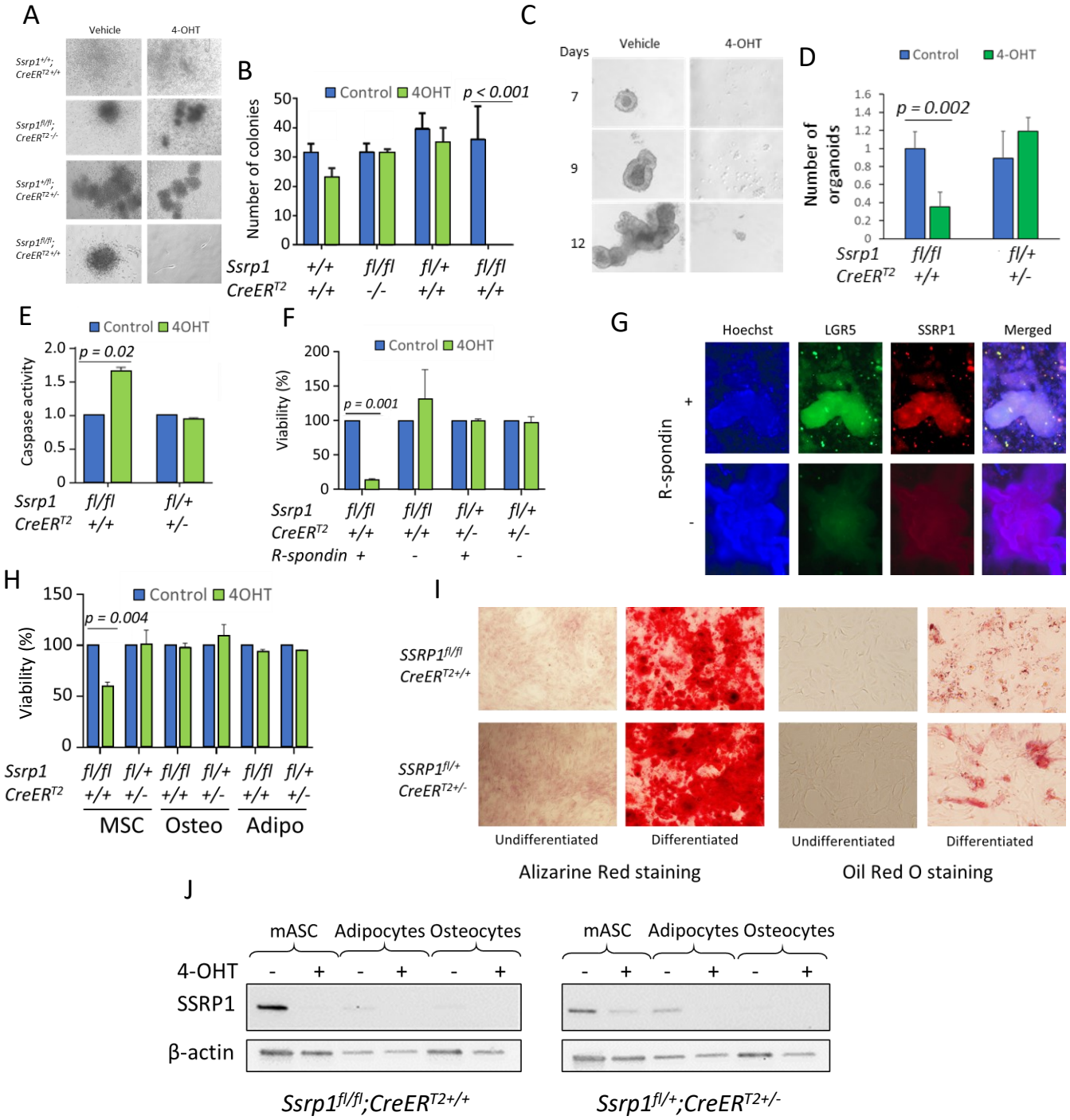
A
Vehicle
4-OHT
Ssrp1+/+; CreERT2+/+
Ssrp1fl/fl; CreERT2-/-
Ssrp1+/fl; CreERT2+/-
Ssrp1fl/fl; CreERT2+/+
B
Control 4OHT
p < 0.001
Number of colonies
Ssrp1 +/+ fl/fl fl/+ fl/fl
CreERT2 +/+ -/- +/+ +/+
C
Days
Vehicle
4-OHT
7
9
12
D
Control 4-OHT
p = 0.002
Number of organoids
Ssrp1 fl/fl fl/+
CreERT2 +/+ +/-
E
Control 4OHT
p = 0.02
Caspase activity
Ssrp1 fl/fl fl/+
CreERT2 +/+ +/-
F
Control 4OHT
p = 0.001
Viability (%)
Ssrp1 fl/fl fl/fl fl/+ fl/+
CreERT2 +/+ +/+ +/- +/-
R-spondin + - + -
G
Hoechst
LGR5
SSRP1
Merged
R-spondin
+
-
H
Control 4OHT
p = 0.004
Viability (%)
Ssrp1 fl/fl fl/+ fl/fl fl/+ fl/fl fl/+
CreERT2 +/+ +/- +/+ +/- +/+ +/-
MSC
Osteo
Adipo
I
SSRP1fl/fl CreERT2+/+
SSRP1fl/+ CreERT2+/-
Undifferentiated
Differentiated
Undifferentiated
Differentiated
Alizarine Red staining
Oil Red O staining
J
mASC
Adipocytes
Osteocytes
4-OHT - + - + - +
SSRP1
β-actin
Ssrp1fl/fl;CreERT2+/+
Ssrp1fl/+;CreERT2+/-

Figure 6

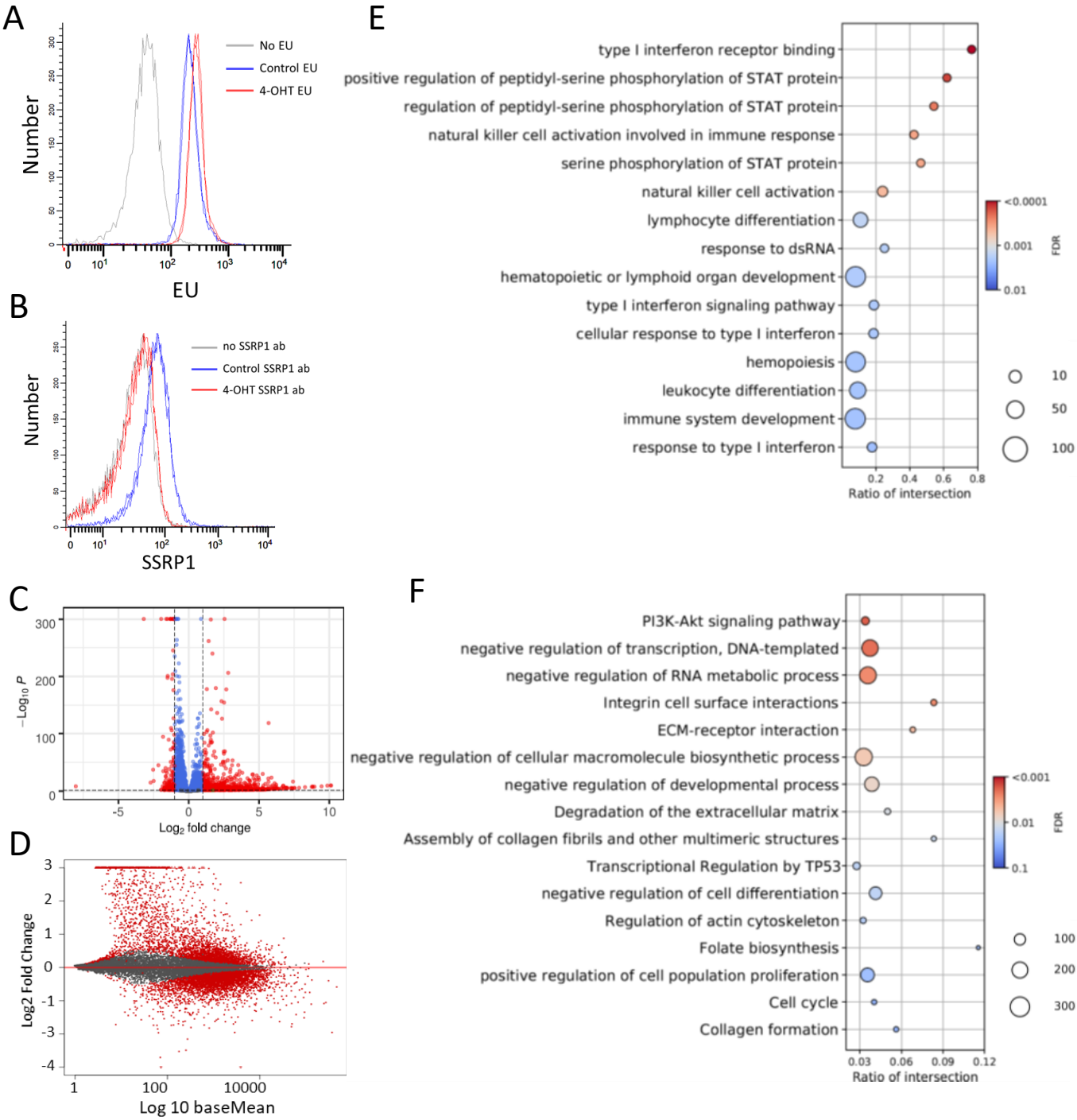
A
No EU
Control EU
4-OHT EU
Number
EU
B
no SSRP1 ab
Control SSRP1 ab
4-OHT SSRP1 ab
Number
SSRP1
C
−Log10 P
Log2 fold change
D
Log2 Fold Change
Log 10 baseMean
E
type I interferon receptor binding
positive regulation of peptidyl-serine phosphorylation of STAT protein
regulation of peptidyl-serine phosphorylation of STAT protein
natural killer cell activation involved in immune response
serine phosphorylation of STAT protein
natural killer cell activation
lymphocyte differentiation
response to dsRNA
hematopoietic or lymphoid organ development
type I interferon signaling pathway
cellular response to type I interferon
hemopoiesis
leukocyte differentiation
immune system development
response to type I interferon
Ratio of intersection
FDR
<0.0001
0.001
0.01
10
50
100
F
PI3K-Akt signaling pathway
negative regulation of transcription, DNA-templated
negative regulation of RNA metabolic process
Integrin cell surface interactions
ECM-receptor interaction
negative regulation of cellular macromolecule biosynthetic process
negative regulation of developmental process
Degradation of the extracellular matrix
Assembly of collagen fibrils and other multimeric structures
Transcriptional Regulation by TP53
negative regulation of cell differentiation
Regulation of actin cytoskeleton
Folate biosynthesis
positive regulation of cell population proliferation
Cell cycle
Collagen formation
Ratio of intersection
FDR
<0.001
0.01
0.1
100
200
300

Figure 7

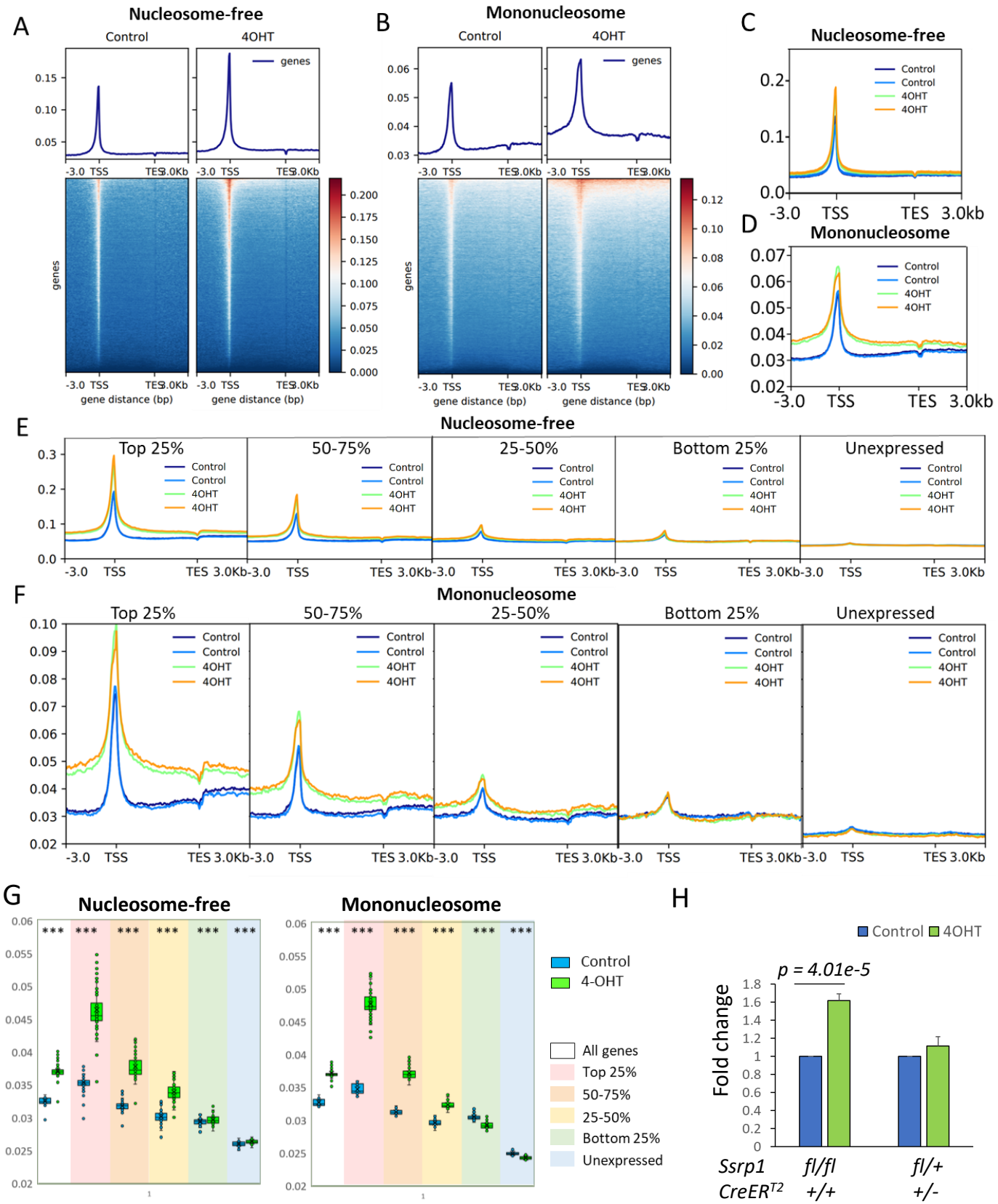
A
Nucleosome-free
Control
4OHT
genes
-3.0 TSS TES 3.0Kb
gene distance (bp)
B
Mononucleosome
C
Nucleosome-free
Control
Control
4OHT
4OHT
D
Mononucleosome
E
Nucleosome-free
Top 25%
50-75%
25-50%
Bottom 25%
Unexpressed
F
Mononucleosome
G
Nucleosome-free
Mononucleosome
Control
4-OHT
All genes
Top 25%
50-75%
25-50%
Bottom 25%
Unexpressed
H
Control 4OHT
p = 4.01e-5
Fold change
Ssrp1 CreER^{T2}
fl/fl +/+
fl/+ +/-

Figure 8

A

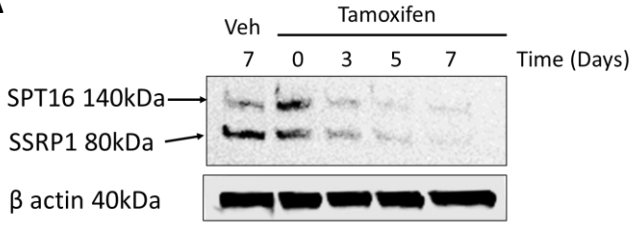

B

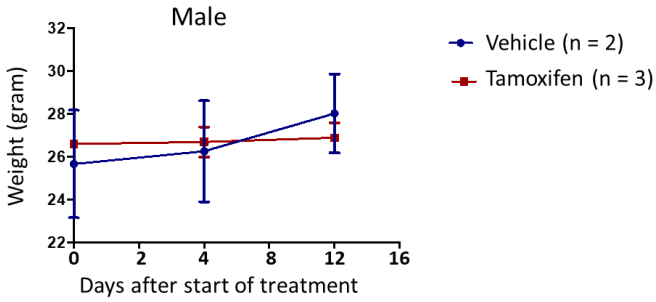

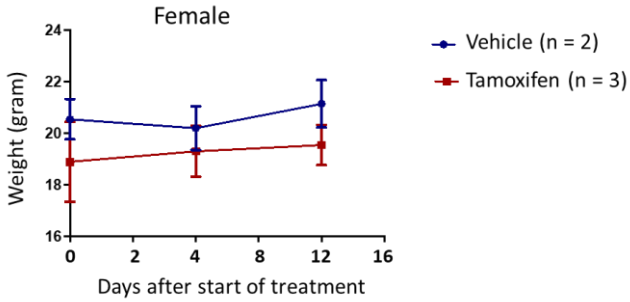

C

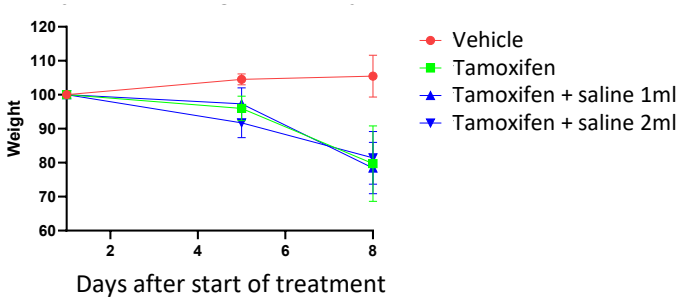

D

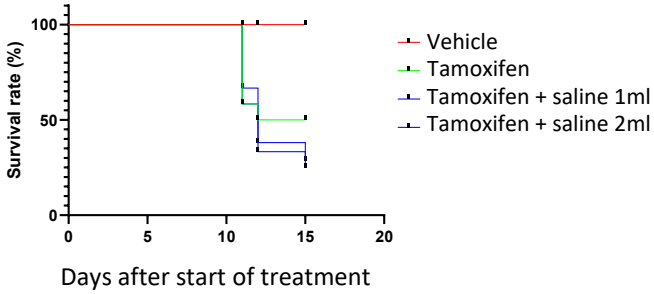

E

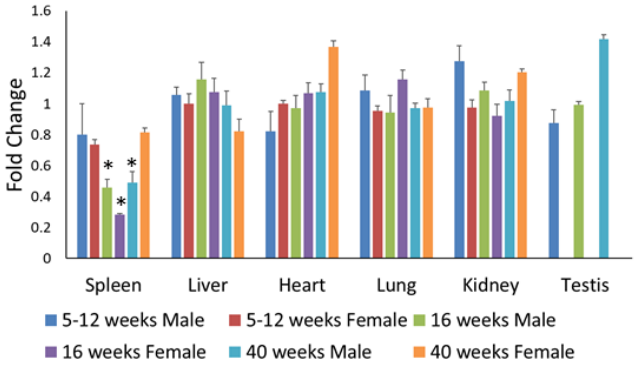

F

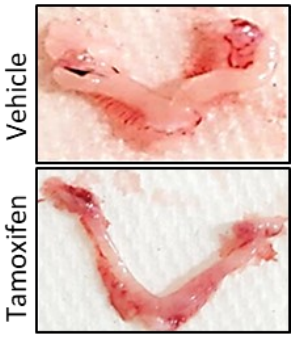

G

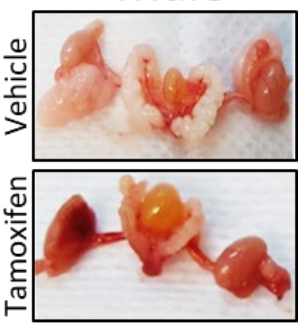

Figure EV1.

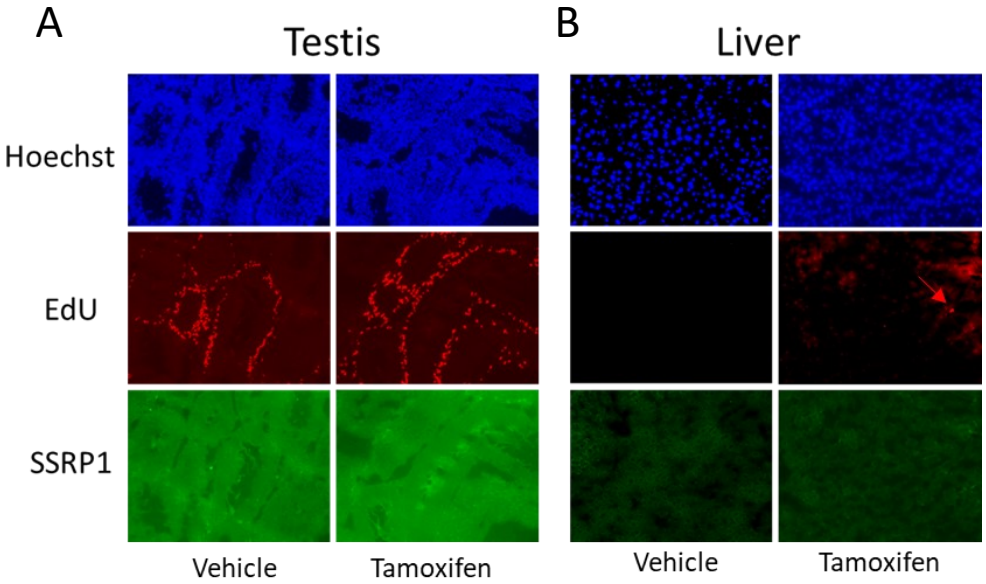
A
Testis
B
Liver
Hoechst
EdU
SSRP1
Vehicle
Tamoxifen
Vehicle
Tamoxifen

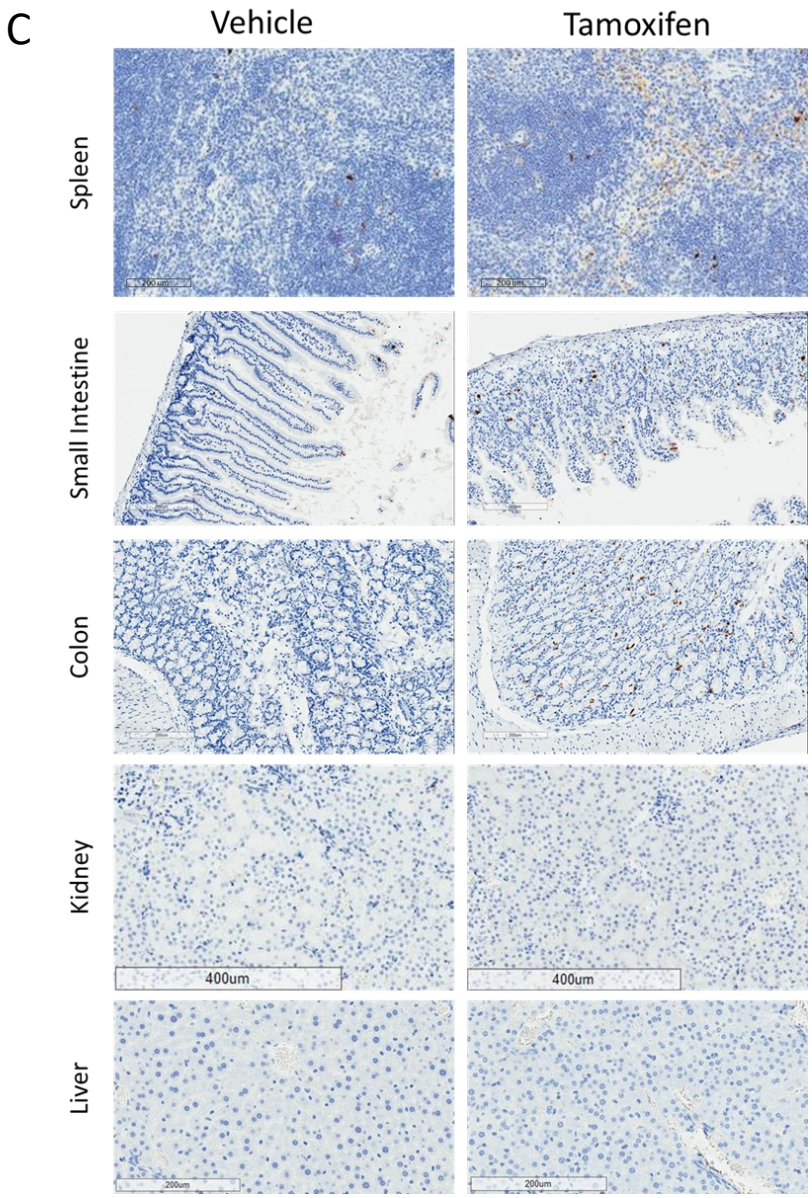
C
Vehicle
Tamoxifen
Spleen
Small Intestine
Colon
Kidney
Liver
400um
400um

Figure EV2.

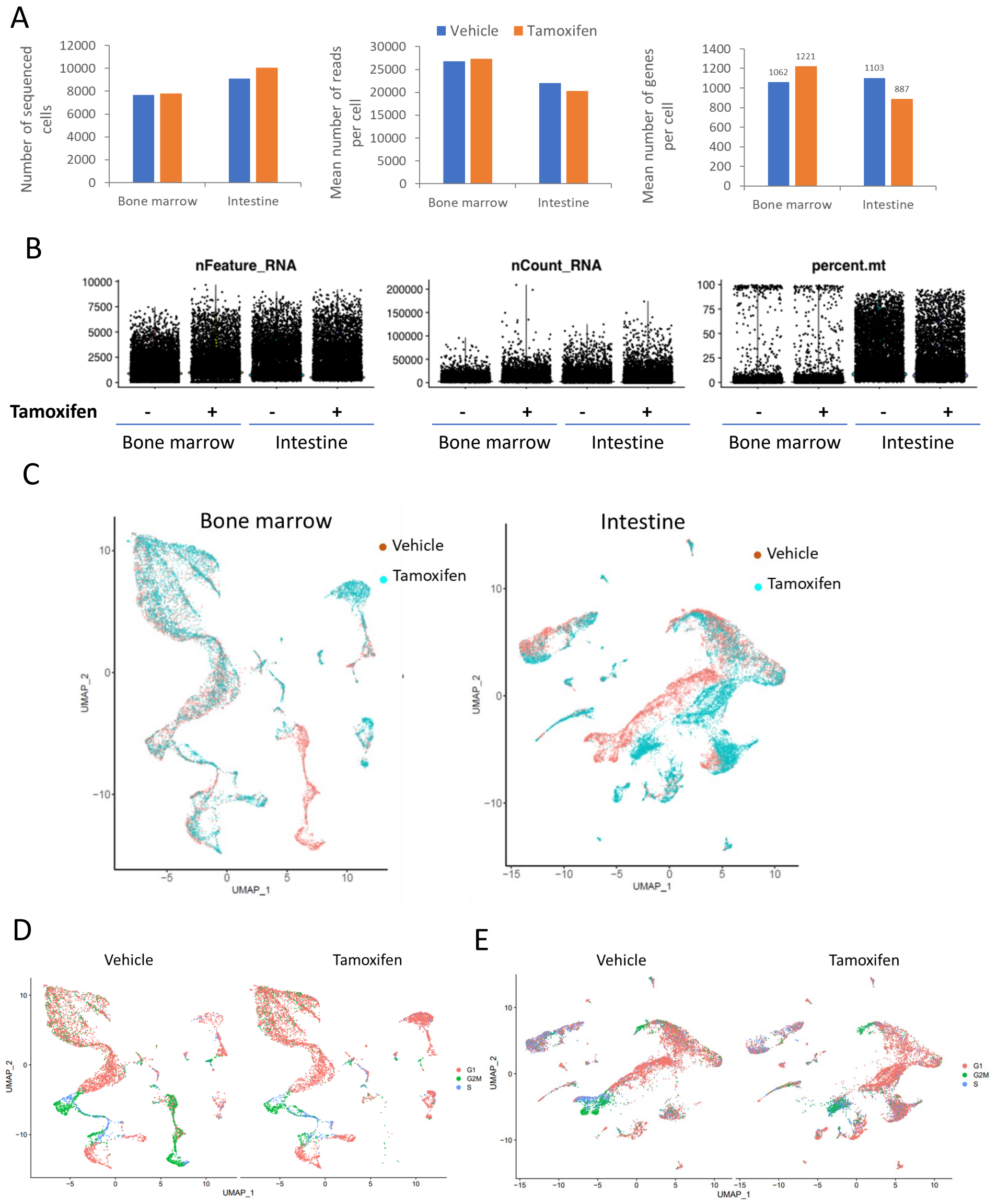
A
Vehicle
Tamoxifen
Number of sequenced cells
Mean number of reads per cell
Mean number of genes per cell
1062
1221
1103
887
Bone marrow
Intestine
B
nFeature_RNA
nCount_RNA
percent.mt
Tamoxifen
C
Bone marrow
Intestine
UMAP_1
UMAP_2
D
E
G1
G2M
S

Figure EV3.

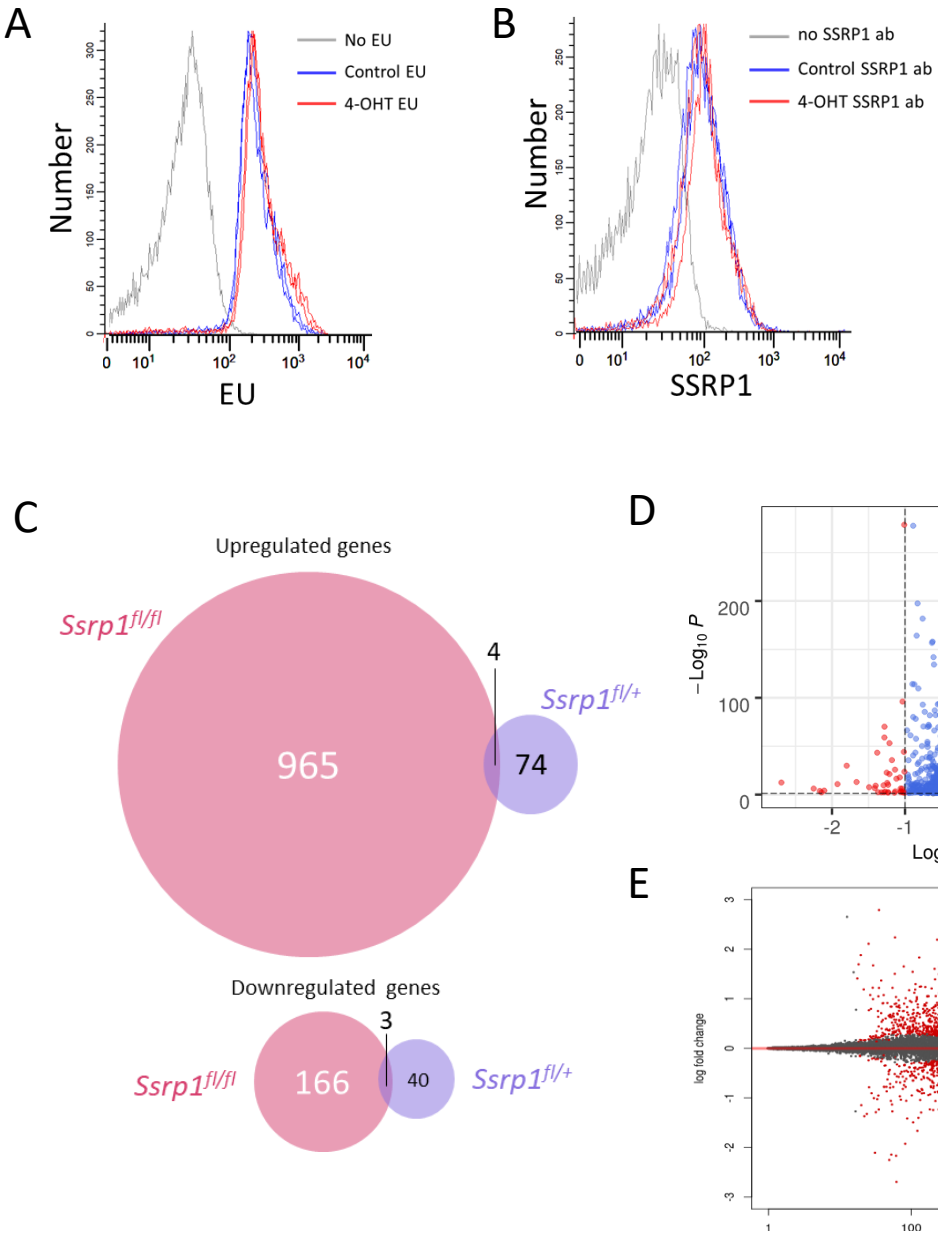
A
No EU
Control EU
4-OHT EU
Number
EU
B
no SSRP1 ab
Control SSRP1 ab
4-OHT SSRP1 ab
Number
SSRP1
C
Upregulated genes
Ssrp1fl/fl
Ssrp1fl/+
965
4
74
Downregulated genes
Ssrp1fl/fl
Ssrp1fl/+
166
3
40
D
−Log10 P
Log2 fold change
E
log fold change

Figure EV4

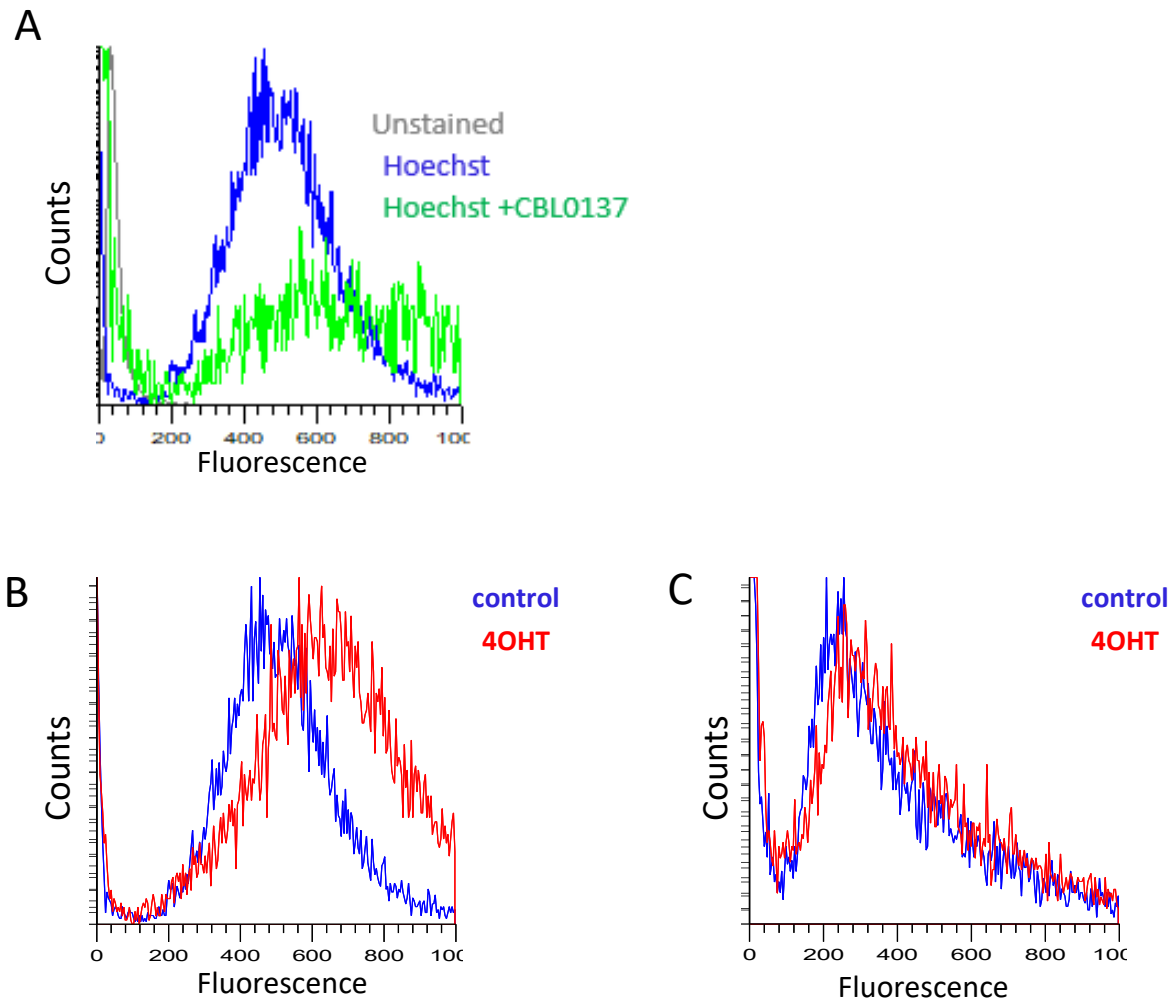
A
Counts
Unstained
Hoechst
Hoechst +CBL0137
200
400
600
800
Fluorescence
B
Counts
control
4OHT
0
200
400
600
800
Fluorescence
C
Counts
control
4OHT
0
200
400
600
800
Fluorescence

Figure EV5.